where $K(k)$ and $E(k)$ are complete elliptic integrals of respectively first and second kind, and the modulus k is defined by

$$k = \sqrt{1-a^2/b^2} \quad . \tag{37}$$

For convenience a table giving the elliptic integrals (Table 4) is included in this report where the angle α is related to k by $\sin\alpha=k$.

Further results for collinear cracks under Mode II loading condition are given in Table 5. In these results the half crack length $(b-a)/2$ is used in normalizing stress intensity factor. $(a/b) = 0$ and $(a/b) = 1$ correspond to the two limiting cases of a single crack of length $2b$ and $b-a$, respectively. As expected $k_1(a)$ becomes unbounded for a 4 and both $k_1(a)$ and $k_1(b)$ approach the corresponding single crack value for $(a/b)\to 1$ (i.e., for a—). An interesting result observed in Fig. 46 and Table 5, however, is that generally for smaller plate thicknesses as a approaches zero the stress intensity factor $k_1(a)$ goes through a minimum before becoming unbounded. This reduction is apparently due to the interaction of the stress fields of the two cracks as the distance $2a$ decreases. For example, from Fig. 47 it may clearly be seen that even though the cleavage stress $\sigma_{22}(x_1,0)$ perpendicular to and on the line of the crack is tensile near the crack and becomes unbounded at the crack tip, it becomes compressive in a certain interval away from the crack. This is largely due to the "bending" effect of the two halves of the plate. Thus after the interaction of stress fields of the two cracks it is seen that the inner crack tips would be in compressive region and consequently there would be some decrease in the stress intensity factor.

4.4 Collinear Cracks Perpendicular to the Boundary

From a viewpoint of interaction between two cracks or between cracks and free boundaries another geometry of great deal of practical interest is that of collinear cracks perpendicular to the plate boundary described in Fig. 48. A special case of this problem is the two surface

4. Tables of Complete Elliptic Integrals K(k) and E(k), k = sinα.

V. Vollständige elliptische Integrale.
V. Complete elliptic integrals.

α	K	E	a	K	E	a	K	E
0°	1,6708	1,5708	50°	1,9356	1,3055	82° 0′	3,3699	1,0278
1°	1,5709	1,5707	51°	1,9539	1,2963	82° 12′	3,3946	1,0267
2°	1,5713	1,5703	62°	1,9729	1,2870	82° 24′	3,4199	1,0256
3°	1,5719	1,6697	53°	1,9927	1,2776	82° 36′	3,4460	1,0245
4°	1,5727	1,5689	54°	2,0133	1,2682	82° 48′	3,4728	1,0234
5°	1,5738	1,5678	55°	2,0347	1,2587	83° 0′	3,5004	1,0223
	1,6761	1,5665	56°	2,0571	1,2492	83° 12′	3,5288	1,0213
	1,6767	1,5650	57°	2,0804	1,2397	83° 24′	3,5581	1,0202
	1,5785	1,5632	58°	2,1047	1,2301	83° 36′	3,5884	1,0192
	1,5805	1,5611	69°	2,1300	1,2206	83° 48′	3,6196	1,0182
	1,5828	1,5589	60°	2,1565	1,2111	84° 0′	3,6518	1,0172
	1,5854	1,5564	61°	2,1842	1,2015	84° 12′	3,6853	1,0163
12°	1,5882	1,5537	62°	2,2132	1,1921	84° 24′	3,7198	1,0153
13°	1,5913	1,5507	63°	2,2435	1,1826	84° 36′	3,7557	1,0144
14°	1,5946	1,5476	64°	2,2754	1,1732	84° 48′	3,7930	1,0135
15°	1,5981	1,5442	65°	2,3088	1,1638	85° 0′	3,8317	1,0127
16°	1,6020	1,5405	66°	2,3439	1,1546	85° 12′	3,8721	1,0118
17°	1,6061	1,5367	67°	2,3809	1,1454	85° 24′	3,9142	1,0110
18°	1,6105	1,5326	68°	2,4198	1,1362	85° 36′	3,9583	1,0102
19°	1,6151	1,5283	69°	2,4610	1,1273	85° 48′	4,0044	1,0094
20°	1,6200	1,5238	70° 0′	2,5046	1,1184	86° 0′	4,0528	1,0087
21°	1,6252	1,5191	70° 30′	2,5273	1,1140	86° 12′	4,1037	1,0079
22°	1,6307	1,5142	71° 0′	2,5507	1,1096	86° 24′	4,1574	1,0072
23°	1,6365	1,5090	71° 30′	2,5749	1,1053	86° 36′	4,2142	1,0065
24°	1,6426	1,5037	72° 0′	2,5998	1,1011	86° 48′	4,2746	1,0059
25°	1,6490	1,4981	72° 30′	2,6256	1,0968	87° 0′	4,3387	1,0053
26°	1,6557	1,4924	73° 0′	2,6521	1,0927	87° 12′	4,4073	1,0047
27°	1,6627	1,4864	73° 30′	2,6796	1,0885	87° 24′	4,4812	1,0041
28°	1,6701	1,4803	74° 0′	2,7081	1,0844	87° 36′	4,5609	1,0036
29°	1,6777	1,4740	74° 30′	2,7375	1,0804	87° 48′	4,6477	1,0031
30°	1,6858	1,4675	75° 0′	2,7681	1,0764	88° 0′	4,7427	1,0026
31°	1,6941	1,4608	75° 30′	2,7998	1,0725	88° 12′	4,8479	1,0022
32°	1,7028	1,4539	76° 0′	2,8327	1,0686	88° 24′	4,9654	1,0017
33°	1,7119	1,4469	76° 30′	2,8669	1,0648	88° 36′	5,0988	1,0014
34°	1,7214	1,4397	77° 0′	2,9026	1,0611	88° 48′	5,2527	1,0010
35°	1,7313	1,4323	77° 30′	2,9397	1,0574	89° 0′	5,4349	1,0008
36°	1,7415	1,4248	78° 0′	2,9786	1,0538	89° 6′	5,5402	1,0006
37°	1,7522	1,4171	78° 30′	3,0192	1,0502	89° 12′	5,6579	1,0005
38°	1,7633	1,4092	79° 0′	3,0617	1,0468	89° 18′	5,7914	1,0005
39°	1,7748	1,4013	79° 30′	3,1064	1,0434	89° 24′	5,9455	1,0003
40°	1,7868	1,3931	80° 0′	3,1534	1,0401	89° 30′	6,1278	1,0002
41°	1,7992	1,3849	80° 12′	3,1729	1,0388	89° 36′	6,3508	1,0001
42°	1,8122	1,3765	80° 24′	3,1928	1,0375	89° 42′	6,6385	1,0001
43°	1,8256	1,3680	80° 36′	3,2132	1,0363	89° 48′	7,0440	1,0000
44°	1,8396	1,3594	80° 48′	3,2340	1,0350	89° 54′	7,7371	1,0000
45°	1,8541	1,3506	81° 0′	3,2553	1,0338	90°	∞	1,0000
46°	1,8692	1,3418	81° 12′	3,2771	1,0326			
47°	1,8848	1,3329	81° 24′	3,2995	1,0313			
48°	1,9011	1,3238	81° 36′	3,3223	1,0302			
49°	1,9180	1,3147	81° 48′	3,3458	1,0290			

Jahnke & Emde, "Tables of Functions"

Table 5. Stress intensity factors in an orthotropic strip containing two identical collinear cracks loaded by uniform crack surface pressure p or shear q; $H_1=H_2=H$, $\kappa=1$, $H\delta/(b-a)/2 = 0.4$.

$\frac{2a}{b-a}$	$\sigma_{22}(x_1,0)=-p$		$\sigma_{12}(x_1,0)=-q$	
	$\frac{k_1(b)}{p(\frac{b-a}{2})^{1/2}}$	$\frac{k_1(a)}{p(\frac{b-a}{2})^{1/2}}$	$\frac{k_2(b)}{q(\frac{b-a}{2})^{1/2}}$	$\frac{k_2(a)}{q(\frac{b-a}{2})^{1/2}}$
0	9.376	∞	2.629	∞
.01	3.693	6.996	2.106	5.837
.1	3.788	2.837	1.952	2.300
.2	3.962	3.113	1.935	1.989
.3	4.074	3.642	1.933	1.939
.4	4.124	3.971	7.933	1.933
.5	4.138	4.103	1.933	1.932
.6	4.141	4.138	1.933	1.933
.7	4.140	4.143	1.933	1.933
.8	4.140	4.142	7.933	1.933
.9	4.139	4.140	1.933	1.933
1	4.139	4.140	1.933	1.933
2	4.142	4.142	1.933	1,933

cracks simulating weld defects on both surfaces.

Some sample results for the stress intensity factors $k(a)$ and $k(b)$ for two symmetrically located collinear cracks are given in Table 6. Fig. 49 shows the results for two (collinear) surface cracks. For very shallow surface cracks (i.e., for $a \to h$), as seen from the figure $k(a)$ approaches the stress intensity factor in a semi-infinite plane containing an edge crack of depth $2a_0$, namely

$$k_1(a) \to 1.586\ \sigma_0\sqrt{a_0} \quad . \tag{38}$$

In the other limiting case for which $a \to 0$, $k(a)$ approaches the stress intensity factor in a symmetrically loaded infinite plane containing

Table 6. Stress intensity factors for collinear internal cracks in a strip (Figure 1, $a_0 = (b-a)/2$).

a/h	b/h	$\frac{k(a)}{\sigma_0\sqrt{a_0}}$	$\frac{k(b)}{\sigma_0\sqrt{a_0}}$
0	0.4	$(\to \infty)$	1.5690
0.1	0.5	1.1746	1.1169
0.2	0.6	1.1102	1.0961
0.4	0.8	1.0984	1.1250
0.5	0.9	1.1290	1.2278
0.6	1.0	1.6080	$(\to \infty)$
0	0.8	$(\to \infty)$	2.5680
0.1	0.9	1.6730	1.7451
0.2	1.0	2.1769	$(\to \infty)$
0.5	0.95	1.1960	1.4711
0.5	0.98	1.2713	1.9008
0.5	1.0	1.6228	$(\to \infty)$

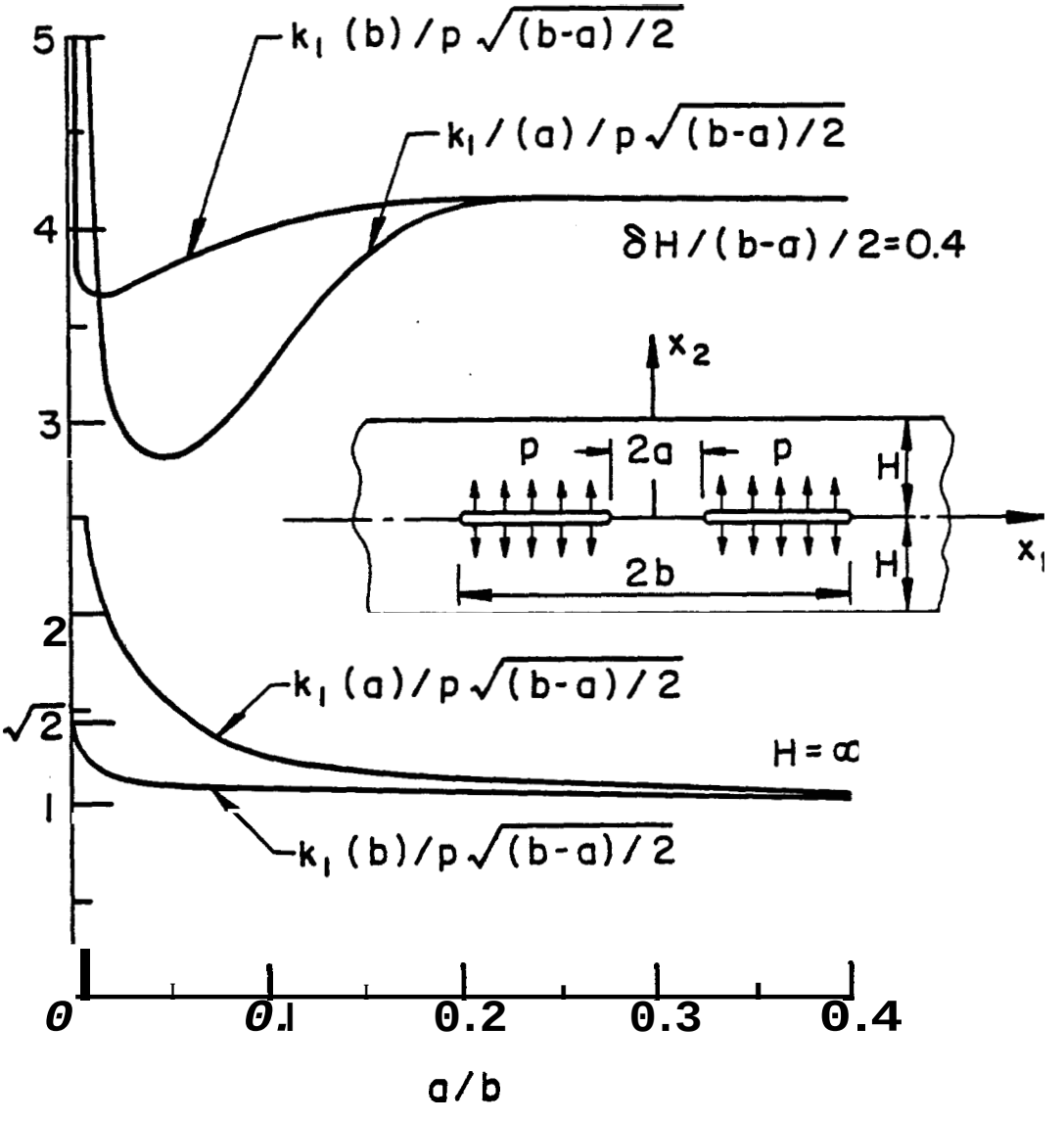

Figure 46. Stress intensity factors for two collinear cracks in an orthotropic strip.

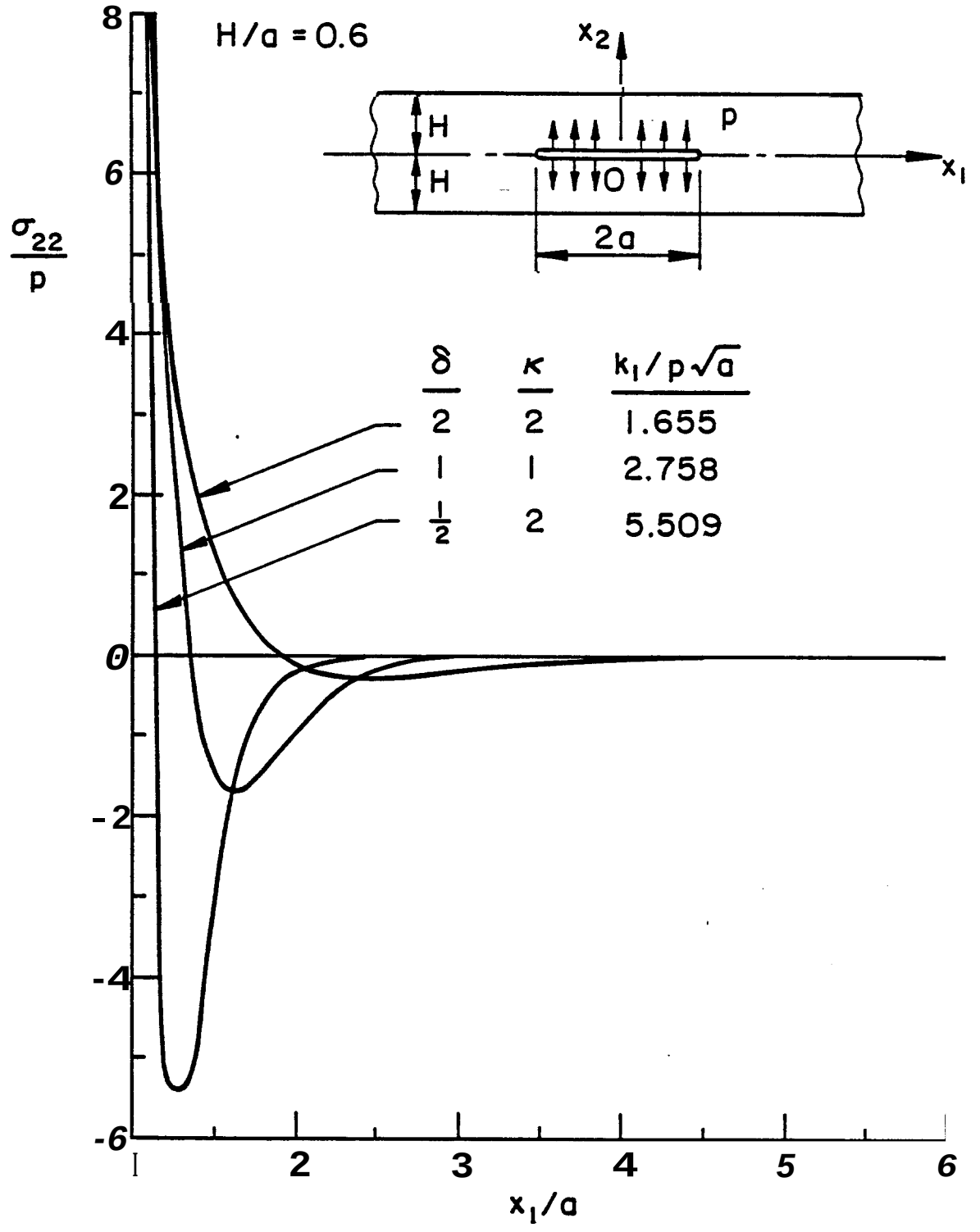

Figure 47. The effect of material orthctropy on the normal stress $\sigma_{22}(x_1,0)$ in a strip containing a pressurized crack ($\delta=\kappa=1$ isotropic strip).

two edge cracks. In this case, if the resultant force perpendicular to the cracks is P, and the length of the net ligament is 2a, it can be shown that the stress state in the net ligament is given by

$$\sigma_{yy}(x,0) = \frac{P}{\pi\sqrt{a^2-x^2}} \quad , \quad \sigma_{xy}(x,0) = 0 \quad . \tag{39}$$

Thus, by observing that

$$P = 2h\sigma_0 = 2a\sigma_1 \tag{40}$$

and

$$k(a) = \lim_{x\to a} \sqrt{2(a-x)}\ \sigma_{yy}(x,0) \quad , \tag{41}$$

we obtain

$$k(a) = \frac{2}{\pi}\ \sigma_1\ \sqrt{a} \quad . \tag{42}$$

These two limiting results are also shown in Fig. 49.

5. INTERACTION BETWEEN FLAT INCLUSIONS AND CRACKS

Few unusual results aside, the problem of interaction between two cracks is relatively well-understood in the sense that the resulting stress field or the stress intensity factors would either be amplified or reduced as the distance between the cracks decreases. Almost in all cases the qualitative nature of the result could be predicted intuitively. For example, if the cracks are parallel then they would be in each other's shadow and there would be a reduction in the stress intensity factors. On the other hand if the cracks are co-planar then one would expect an amplification in the stress intensity factors, The exception or the unusual result in this case is the reduction in the stress

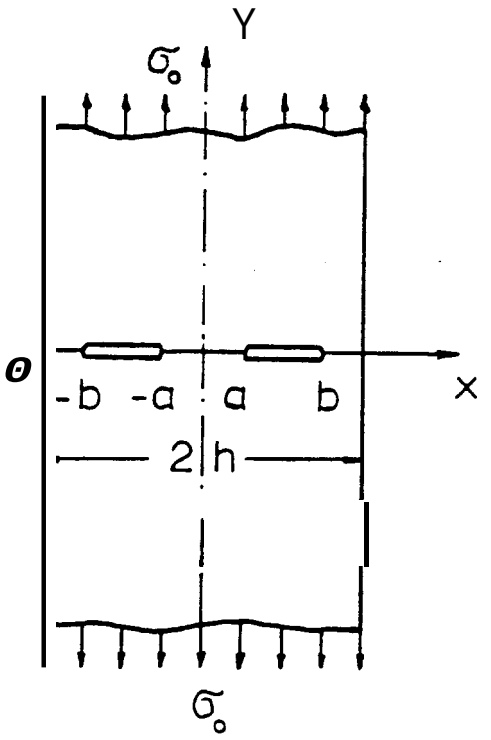

Figure 48. Infinite strip with two internal cracks.

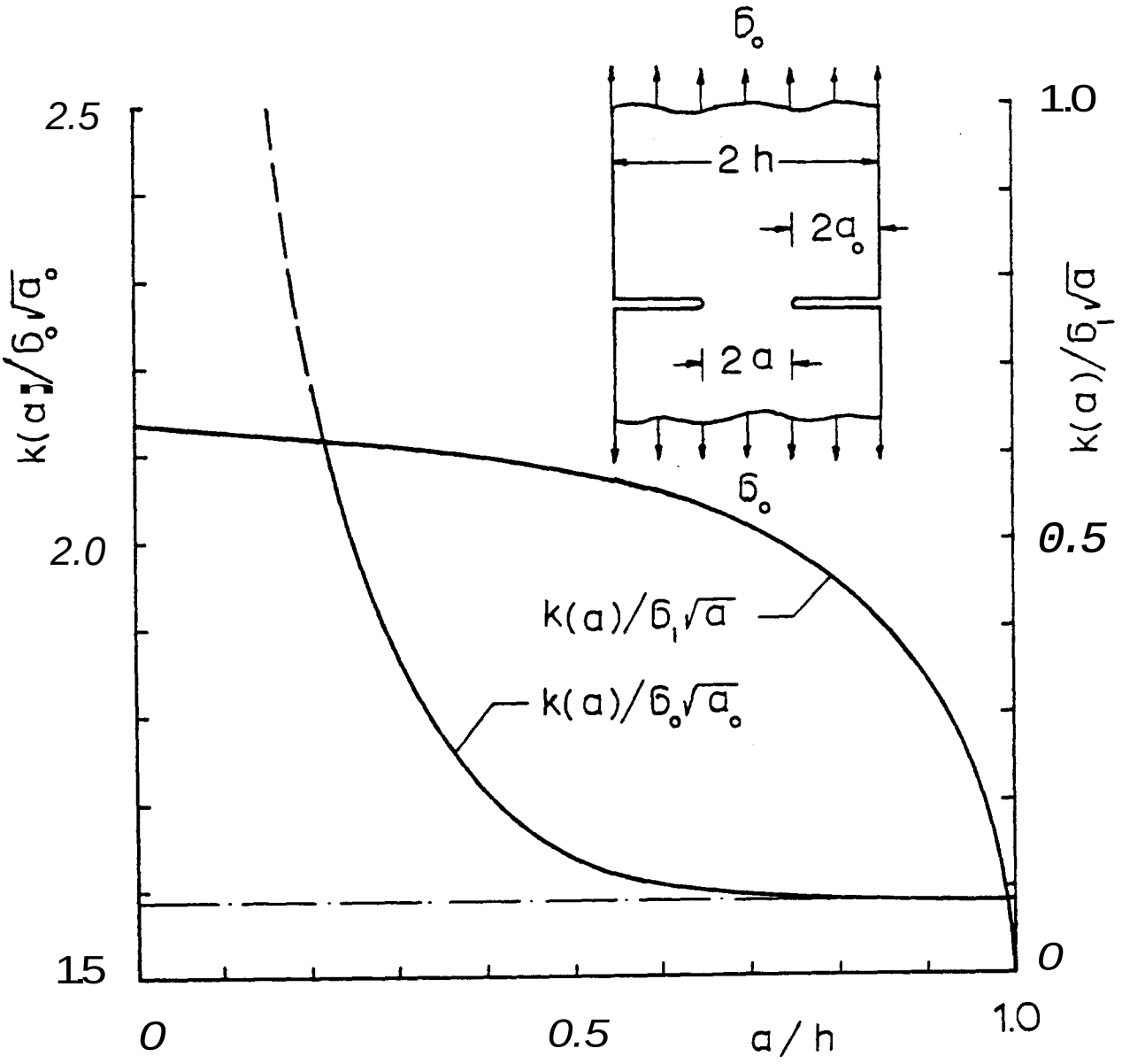

Figure 49. The stress intensity factor **for the edge cracks** in **an infinite strip** ($\sigma_1 = \sigma_0 h/a$).

intensity factors at the inner crack tips for certain relative crack locations in plates with relatively smaller thicknesses. Some specific problems relating to interaction between cracks were discussed in the previous sections.

Intuitively what is not as well understood is the problem of interaction between cracks and flat inclusions. Separately both flaws have singular stresses and consequently are locations for potential fracture initiation. However, the inclusions are also "stiffeners" and therefore, properly oriented, they should tend to arrest crack propagation. For this reason in this study it is found to be worthwhile to undertake a detailed investigation of the problem on which the technical literature seems to be extremely weak. Particularly interesting in this problem is the behavior of the stress state around the ends of the inclusions and at the points of intersection between inclusions and cracks. The details of the analysis of this crack-inclusion interaction problem and very detailed results are given in Appendix A of this report.

6. PLANAR CRACKS OF FINITE SIZE

Referring to Fig. 50 which is reproduced from API Standard 1104 and which describes a set of empirical rules regarding the interaction between planar cracks it may be seen that somewhat more quantitative results are needed. The general method to provide such results is described in Appendix B of this report. The appendix gives the results only for a single internal crack. However, the method is general and will be used for the interaction of coplanar surface cracks, and coplanar internal cracks located parallel or in series.

		INTERACTION EXISTS IF:	IF INTERACTION EXISTS EFFECTIVE FLAW SIZE IS:
CASE 1	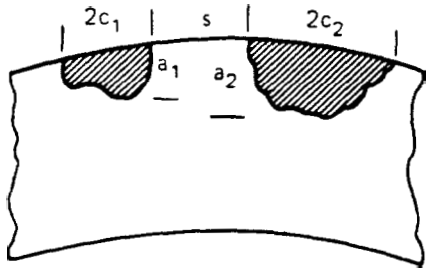	$s < c_1 + c_2$	$a_e = a_2$ $2c_e = 2c_1 + s + 2c_2$
CASE 2	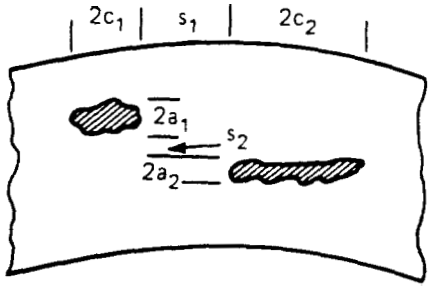	$s_1 < c_1 + c_2$ and $s_2 < a_1 + a_2$	$2a_e = 2a_1 + s_2 + 2a_2$ $2c_e = 2c_1 + s_1 + 2c_2$
CASE 3	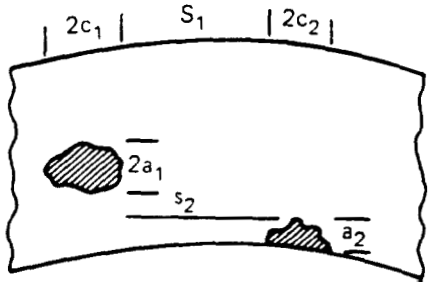	$s_1 < c_1 + c_2$ and $s_2 < a_1 + \frac{a2}{2}$	$a_e = 2a_1 + s_2 + a_2$ $2c_e = 2c_1 + s_1 + 2c_2$
CASE 4	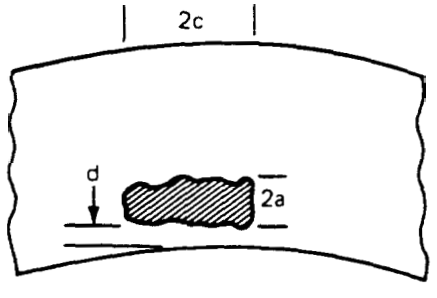	$d < a$	$a_e = d + 2a$ $2c_e = 2c$
CASE 5	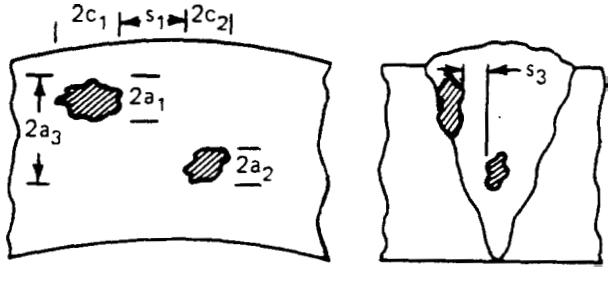	$s_1 < c_2 + c_2$ and $s_3 < a_1 + a_2$	$2a_e = 2a_3$ $2c_e = 2c_1 + s_1 + 2c_2$

Fig. 50. RULES FOR EVALUATION OF FLAW INTERACTION

7. REFERENCES FOR PART I

1. C.D. Lundin, "The Significance of Weld Discontinuities - A Review of Current Literature", W.R.C. Bulletin, No. 222, Dec. 1976.

2. "Proposed Assessment Methods for Flaws with Respect to Failure by Brittle Fracture", Welding in the World, Vol. 13, No. 1/2, 1975.

3. S.T. Rolfe and J.M. Barsom, Fracture and Fatique Control in Structures, Prentice Hall, 1977.

4. Fatigue Crack Propagation, ASTM-STP 415, 1967.

5. M.S. Kamath, "The COD Design Curve: An Assessment of Validity Using Wide Plate Tests", The Welding Institute Research Report 71/1978/E, Sept. 1978.

6. J.D. Harrison, "The 'State-of-the-Art' in Crack Tip Opening Displacement Testing and Analysis", the Welding Institute Research Report 108/1980, April 1980.

7. J.D. Harrison, M.G. Dawes, G.L. Archer, and M.S. Kamath, "The COD Approach and Its Application to Welded Structures", ASTM-STP668, 1979.

8. F. Erdogan, "Theoretical and Experimental Study of Fracture in Pipelines Containing Circumferential Flaws", Final Report, DOT-RSPA-DMA-50/83/3, Sept. 1982.

9. V.L. Hein and F. Erdogan, "Stress Singularities in a Two-Material Wedge", Int. J. of Fracture Mechanics, Vol. 7, pp. 317-330, 1971.

10. F. Erdogan, G.D. Gupta and M. Ratwani, "Interaction Between a Circular Inclusion and an Arbitrarily Oriented Crack", J. Appl. Mech., Vol. 41, Trans. ASME, pp. 1007-1013, 1974.

11. F. Erdogan and G.D. Gupta, "The Inclusion Problem with a Crack Crossing the Boundary", Int. J. of Fracture, Vol. 11, pp. 13-27, 1975.

12. F. Erdogan and G.C. Sih, "On the Crack Extension in Plates Under Plane Loading and Transverse Shear", J. Basic Engng., Trans. ASME, Vol. 85, pp. 519-526, 7963.

13. N.I. Muskhelishvili, Some Basic Problems of the Mathematical Theory of Elasticity, P. Noordhoff Ltd. Groningen-Holland, 1953.

14. T.S. Cook and F. Erdogan, "Stresses in Bonded Materials with a Crack Perpendicular to the Interface", Int. J. Engng. Sci., Vol. 10, pp. 667–697, 1972.

15. F. Erdogan and V. Biricikoglu, "Two Bonded Half Planes with a Crack Going Through the Interface", Int. J. Engng. Sci., Vol. 11, pp. 745–766, 1973.

16. F. Erdogan and T.S. Cook, "Antiplane Shear Crack Terminating at and Going Through a Bimaterial Interface", Int. J. of Fracture, Vol. 10, pp. 227–240, 1974.

17. J.L. Bassani and F. Erdogan, "Stress Intensity Factors in Bonded Half Planes Containing Inclined Cracks and Subjected to Antiplane Shear Loading", Int. J. Fracture, Vol. 15, pp. 145–158, 1979.

PART II

MECHANISMS OF CORROSION FATIGUE IN PIPELINE STEELS

In this part, the initial results of studies, designed for developing mechanistic understanding of corrosion fatigue, are described. These studies provide the scientific bases for guiding the development of methodology for assessing safety and durability of pipelines in service, and for guiding the development of improved materials and protection systems. The results are not intended for use directly in design and rule-making.

1. INTRODUCTION

Transmission and distribution pipelines are exposed to a broad range of chemical environments, both in terms of corrosive species that are present in soils (such as carbonates, chlorides and nitrates) and of deleterious species that may be transported within the lines (such as hydrogen and ammonia, and hydrogen sulfide and water/water vapor as impurities in natural gas and oil). These environments, acting in concert with operating stresses (both static and cyclic stresses) and residual stresses, can cause cracks to initiate and grow, and result in subsequent failure (leakage or rupture). In addition to these external environments, hydrogen that might be present in the steel (introduced during fabrication, processing or field installation, or by corrosion or cathodic charging during service) can also lead to cracking. Quantitative information and understanding are needed, therefore, to assess the safety and reliability of pipelines during service, and to guide in the development of improved materials and protection systems.

Although a considerable amount of research has been devoted to the problems of environmentally assisted cracking in pipeline steels, most of this effort, however, has been directed to the study of stress corrosion cracking (or cracking under static loading) and of corrosion per se. For a range of reasons, quantitative understanding of the phenomenological and mechanistic aspects of environmentally assisted cracking is yet to be fully developed. Research during recent years, at Lehigh University and elsewhere, has shown that environmentally assisted cracking results from

the interaction of clean metal surfaces (produced by cracking or by deformation) with the environment, and that the very early stages (i.e., the first few milliseconds to few seconds) of reactions are responsible for the enhanced cracking. Fatigue (associated with cyclic loading from a variety of sources), being a proficient mechanical process for creating new surfaces, acting in concert with corrosion, therefore, may be a more serious failure mechanism than stress corrosion cracking.

The need to consider corrosion fatigue as a potentially significant failure mechanism in pipelines is based on the recognition that the operating pressure (or stresses) do not remain truly constant and minor fluctuations in stresses can significantly alter cracking response [1-4]. Indeed, it has been difficult to reconcile service failures and laboratory stress corrosion cracking data without allowing for the possibility for corrosion fatigue [4,5]. To properly address the problems of corrosion fatigue, it is essential to recognize the multi-faceted nature of the phenomenon which reflects the synergism of chemistry/electrochemistry, mechanics and metallurgy. The cracking response reflects both the nature and the kinetics of chemical reactions between the environment and the fresh crack surfaces, and the interactions of hydrogen that is produced by these reactions with the microstructure [6]. Significant advances in understanding and in placing corrosion fatigue analysis on a fundamentally sound and quantitative basis depends on the understanding of the mechanisms for and various processes that control corrosion fatigue.

2. PROGRAM OBJECTIVE AND SCOPE

In this part of the program, a multi-disciplinary research is being undertaken to investigate the mechanisms of corrosion fatigue crack initiation and propagation in pipeline steels exposed to aqueous environments. The program is directed at (1) the development of quantitative understanding of the early stage of chemical reactions in relation to the crack initiation and propagation, (2) elucidating the mechanisms for corrosion fatigue crack initiation and propagation, including the influences of chemical, mechanical and metallurgical variables, and

(3) the formulation and evaluation of models for predicting cracking response and service performance. A combined fracture mechanics, surface chemistry and material science approach is used.

The specific areas of research are as follows:

(1) Determination of the kinetics of passivation (viz., initial reactions) as functions of temperature, pH, ion concentration, and other factors.

(2) Determination of the kinetics of fatigue crack initiation as a function of temperature for selected environmental conditions, and correlation with the chemical data.

(3) Determination of the kinetics of fatigue crack propasation as a function of temperature for selected environmental conditions, and correlation with the chemical data.

(4) Examination of the influences of loading variables (such as cyclic load frequency, waveform, and load ratio) on corrosion fatigue crack initiation and propagation.

(5) Synthesis of chemical, mechanical and metallurgical data to develop quantitative understanding of the mechanisms for corrosion fatigue crack initiation and propagation. Formulation and verification of models for predicting cracking response and service performance.

The research program is planned for a period of three (3) years, and complements an ongoing study on the mechanisms for corrosion fatigue in high-strength steels and titanium alloys sponsored by the Office of Naval Research. Principal efforts during the first year are being directed towards the measurements of the kinetics of passivation and of the kinetics of fatigue crack growth in one electrolyte over a range of temperatures from 10°C to 90°C. Cyclic load frequencies from 10^{-2} to 10 Hr. will be used for the fatigue crack growth experiments. X-70 steel (in plate form) and 1N Na_2CO_3 - 1N $NaHCO_3$ solution are used in these initial studies. Other environments will be considered for later studies,

3. PROGRESS TO DATE

Because of the relatively late starting date of this program with respect to Lehigh's academic calendar, a suitable graduate student was assigned at the beginning of the spring semester (that is, in January,

1983). Principal effort has been directed towards the exploration and development of electrochemical measurement techniques for determining the kinetics of passivation or surface reaction of clean surfaces. Studies of the kinetics of corrosion fatigue crack growth in the X-70 steel have been initiated also. The results are summarized briefly here.

3.1 Electrochemical Measurement Techniques

Two electrochemical measurement techniques are being considered. The first one (the potential step technique) involves cathodically polarizing a "clean" surface at a suitable potential in the electrolyte of interest, suddenly switching to another potential, and monitoring the current transient under potentiostatic conditions at the new potential. The second technique, proposed by Gunchoo Shim as a part of an ONR sponsored program, measures the galvanic current between a cathodically "cleaned" surface and a surface that has been "oxidized" in the electrolyte. The current flow in each of these cases *is* expected to contain information on the reactions of a clean surface with the electrolyte.

Since the second technique more closely simulates the reactions at the crack tip, under open circuit conditions, further evaluation of this technique is being made (in part by Professor Wei in conjunction with his sabbatical leave at EXXON Corporate Research Laboratories during the 1982-83 academic year). The essential elements of this technique are illustrated in Fig. 1. Figure la illustrates the cleaning arrangement, and Fig. 1b, the measurement configuration. Evaluation *of* the technique was carried out using a borate solution, containing an equivolume mixture of 0.15N $Na_2B_4O_7 \cdot 10H_2O$ and 0.15N H_3BO_3 solutions, with pH = 8.8 at room temperature.

An idealized galvanic current transient is illustrated in Fig. 2. The initial rapid decay represents dissipation of charges in the Helmholtz (or double) layer formed during cathodic cleaning. The slower decay represents charge transfer associated with the surface reactions. A simple, linear relationship in log (current) versus time coordinates would suggest a simple first order reaction of the Langmuir type, A typical current transient for iron in a deaerated buffered borate

solution (pH = 8.8) at room temperature is shown in Fig. 3. With increases in test temperature, the current decay becomes more rapid and is consistent with the expected increase in the rates of reactions. It is clear, however, that the processes are much more complex.

To better understand the processes that might contribute to the galvanic current transient, experiments were carried out using only graphite electrodes, In a well-deaerated solution, the current decays rapidly, Fig. 4. This rapid decay is consistent with the expected rapid initial dissipation of the double layer. With the presence of dissolved oxygen, dissipation of the double layer is followed by a much slower current decay, Fig. 5. This slower decay is believed to result from the reduction of oxygen in solution. Other processes, such as the oxidation of iron from Fe^{2+} to Fe^{3+}, are also expected to contribute to the current flow.

Nevertheless, the results are very encouraging. Additional experiments using gold electrodes in 3% NaCl solution have been carried out to attempt to identify the various reactions. Analysis of these data are in progress. Measurements of the reactions of X-70 steel with 1N Na_2CO_3 - 1N $NaHCO_3$ solution will be made to correlate the kinetics of these reactions to corrosion fatigue crack growth response.

3.2 Fatigue Crack Growth

Fatigue crack growth experiments have been carried out on X-70 steel in distilled water, under constant-K conditions at four temperatures from about 20°C to 90°C (Fig. 6). The results clearly show the influence of test frequency and temperature on the rate of corrosion fatigue crack growth. The observed response is similar to that of HY130 steel in distilled water [6]. A stronger temperature dependence for the mechanical component of fatigue crack growth, however, is suggested by these data. Room temperature fatigue crack growth data, obtained in 1N Na_2CO_3 - 1N $NaHCO_3$ solution, are shown in Fig. 7. The result indicates no effect of frequency over the range 0.03 to 10 Hz in this environment. Additional tests at higher temperatures are in progress. The results

will be correlated with the planned electrochemical measurements to develop an understanding of corrosion fatigue crack growth response in this steel.

4. PLANNED RESEARCH

Further development and evaluation of the electrochemical measurement techniques and measurements of the kinetics of reactions of X70 steel with 1N Na_2CO_3 - 1N $NaHCO_3$ and 3.5% NaCl solutions will be made during the coming year. Corrosion fatigue crack growth experiments will be continued to assess the influences of frequency and temperature in the same solutions.

REFERENCES FOR PART II

1. R.R. Fessler and T.J. Barlo, "The Effect of Cyclic Loading on the Threshold Stress for Stress Corrosion Cracking in Mild and HSLA Steels", presented at the ASME Third National Congress on Pressure Vessel and Piping Technology, San Francisco, 1979.

2. O. Vosikovsky and R.J. Cooke, Int. J. Pres. Ves. & Piping, Vol. 6, 1978, pp. 113-129.

3. R.N. Parkins and B.S. Greenwell, Aug./Sept. Metal Science, 1977, pp. 405-413.

4. "Environmentally Induced Cracking of Natural Gas and Liquid Pipelines", Vols. 1 & 2, Final Report, Contract #DOT-OS-60519, ASL Engineering, Inc., 495 South Fairview Ave., Goleta, CA 33017, Dec. 1977.

5. "Proceedings - 5th Symposium on Line Pipe Research", American Gas Association, Cat. No. L30174, 1974.

6. R.P. Wei and Gunchoo Shim, "Fracture Mechanics and Corrosion Fatigue", in Corrosion Fatigue, ASTM STP 801, T.W. Crooker and B.N. Leis, eds., American Society for Testing and Materials, Philadelphia, Pa, 1983, pp. 5-25.

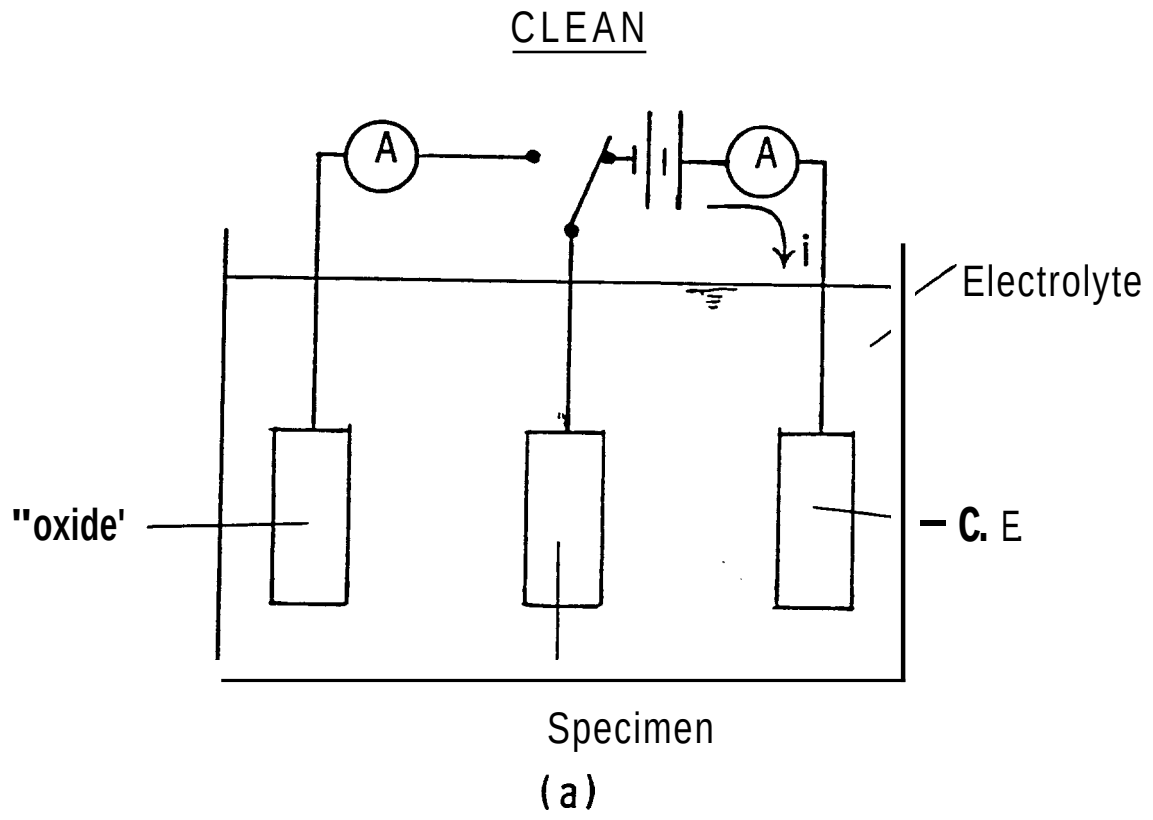

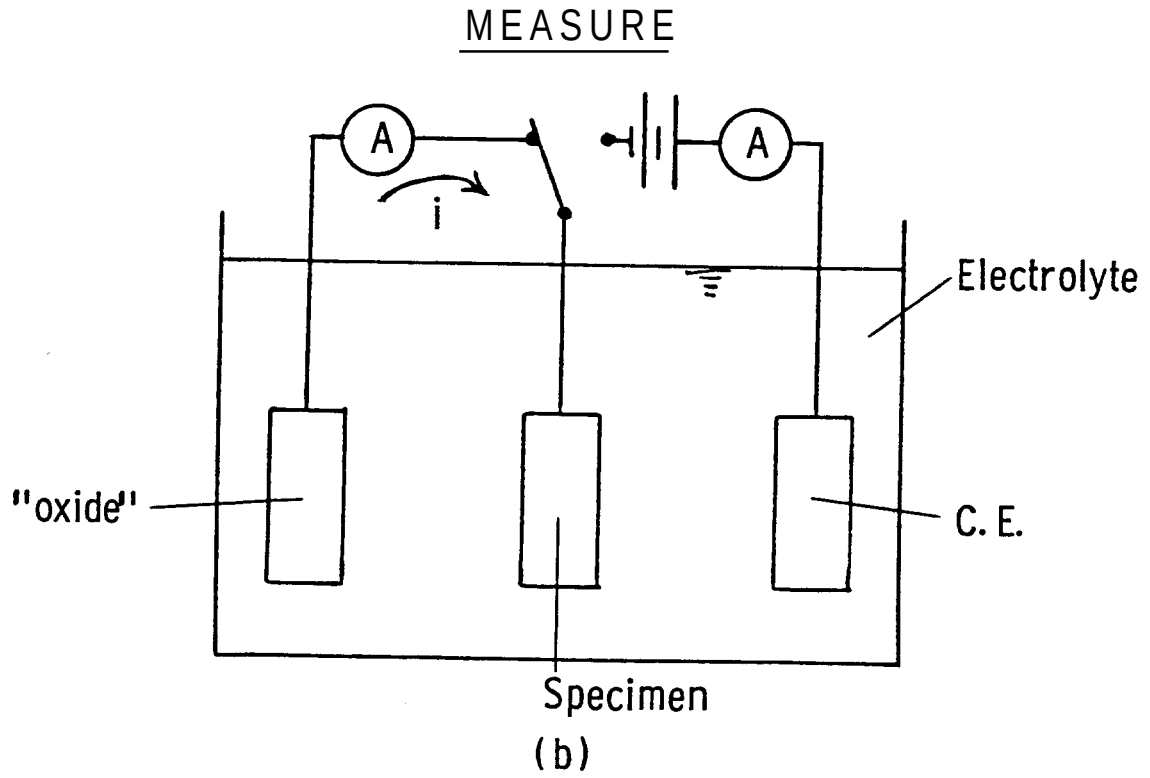

Fig. 1: Schematic illustration of technique for measuring galvanic current transient between "clean" and "oxidized" metal surfaces.

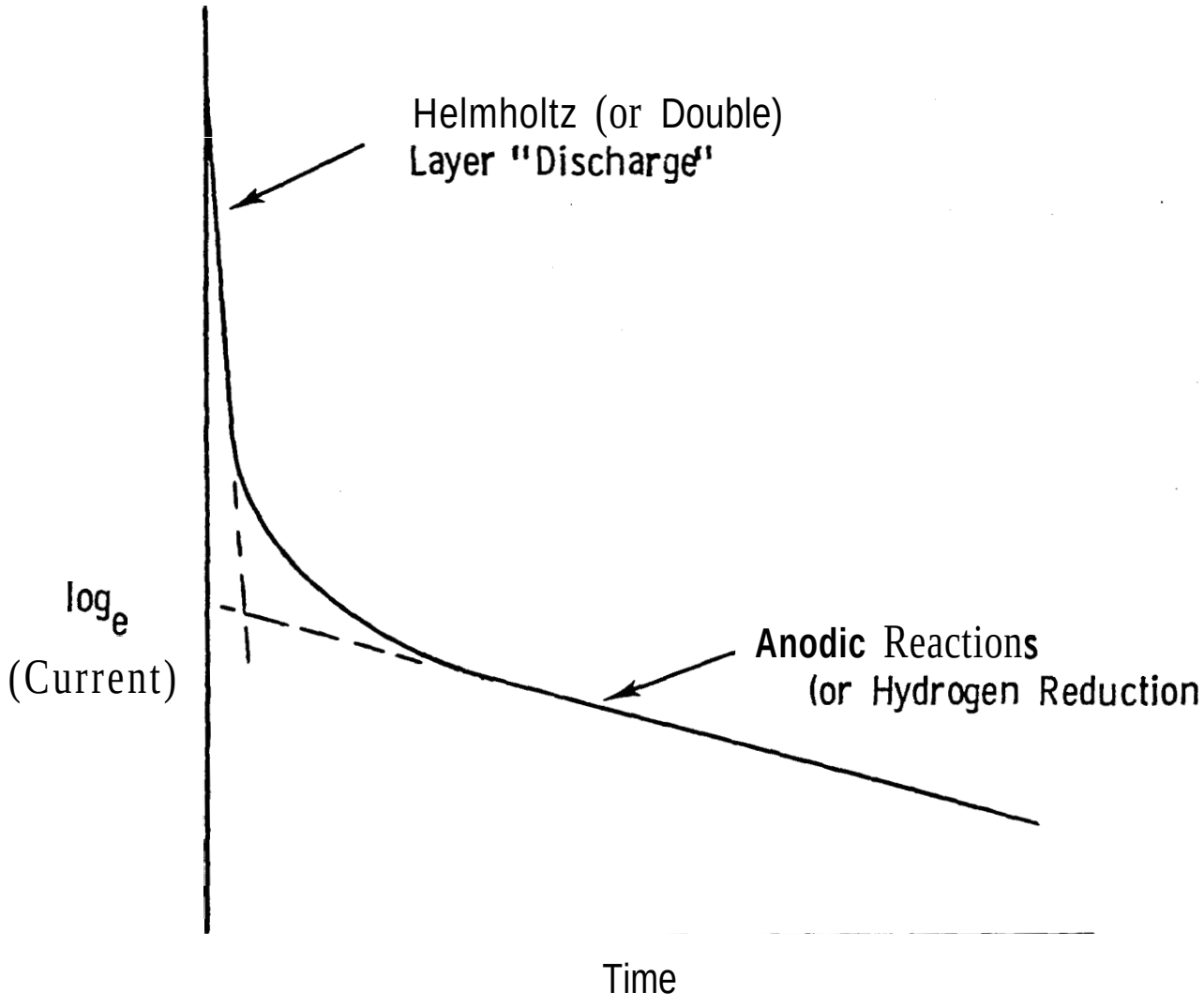

Fig. 2: Idealized galvanic current **transient.**

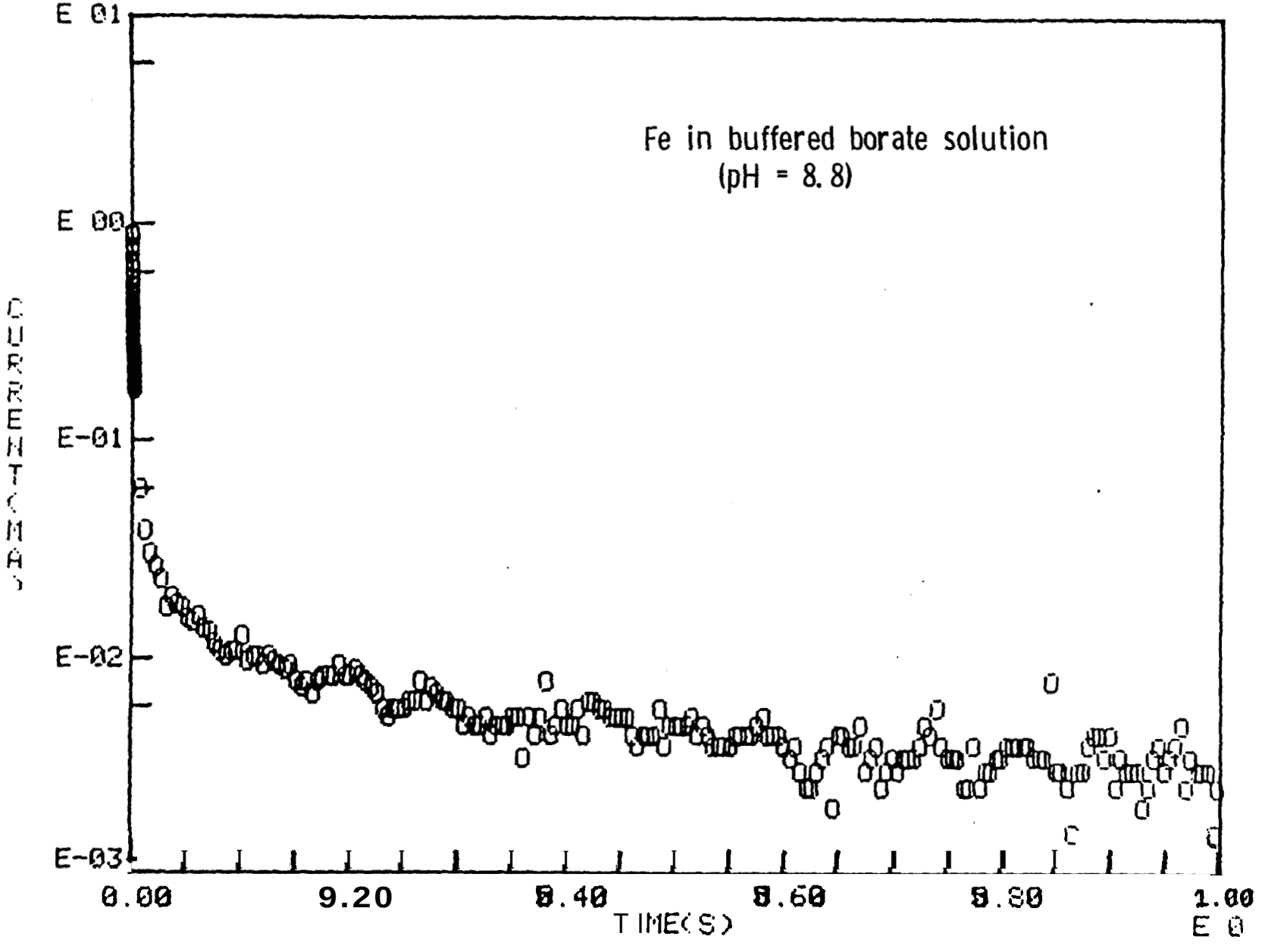

Fig. 3: Typical galvanic current transient for iron in a deaerated buffered borate solution (pH = 8.8) at room temperature.

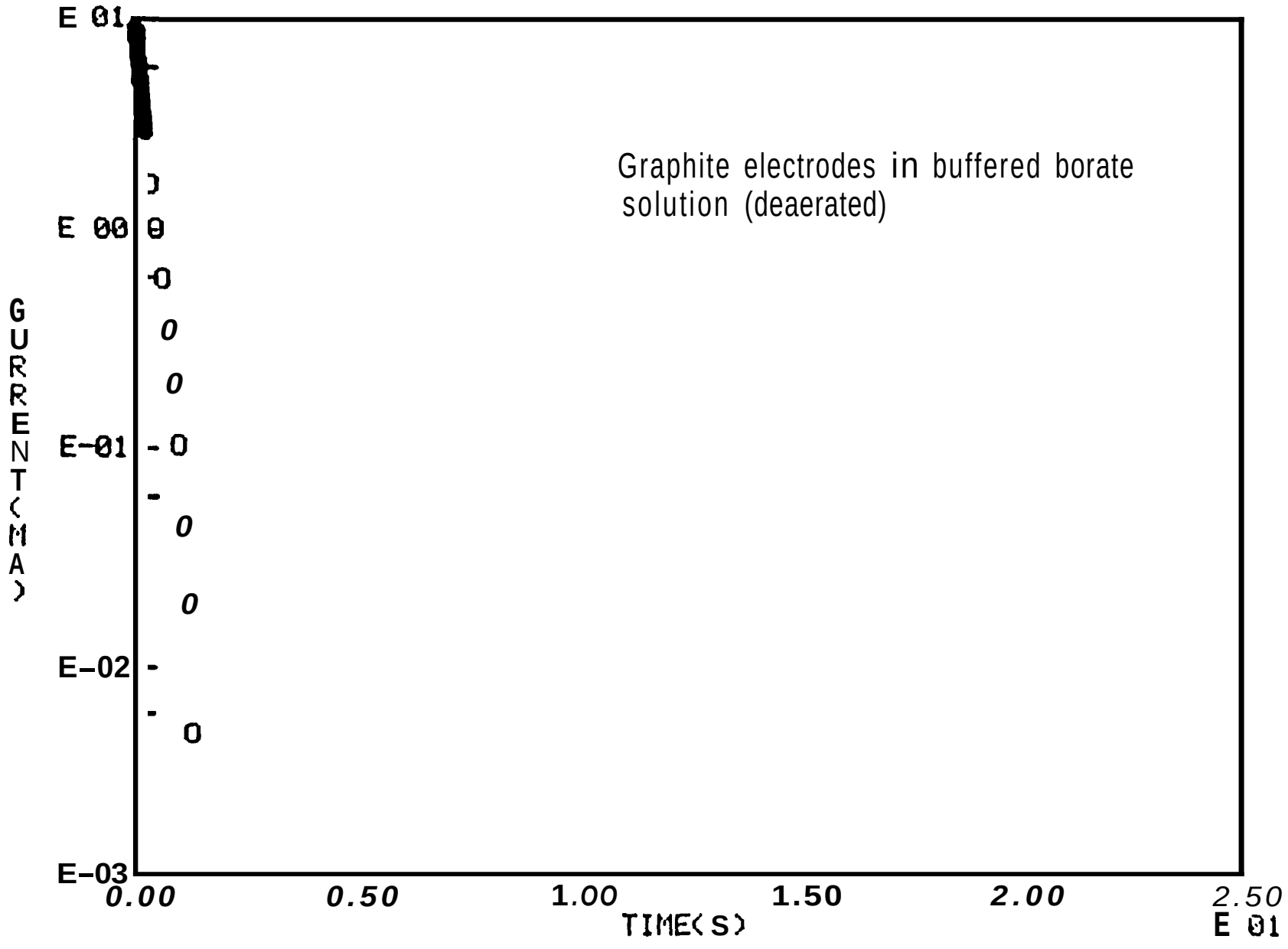

Fig. 4: Typical galvanic current transient between graphite electrode in a deaerated buffered borate solution (pH = 8.8) at room temperature. The transient is associated with dissipation of the Helmholtz (double) layer.

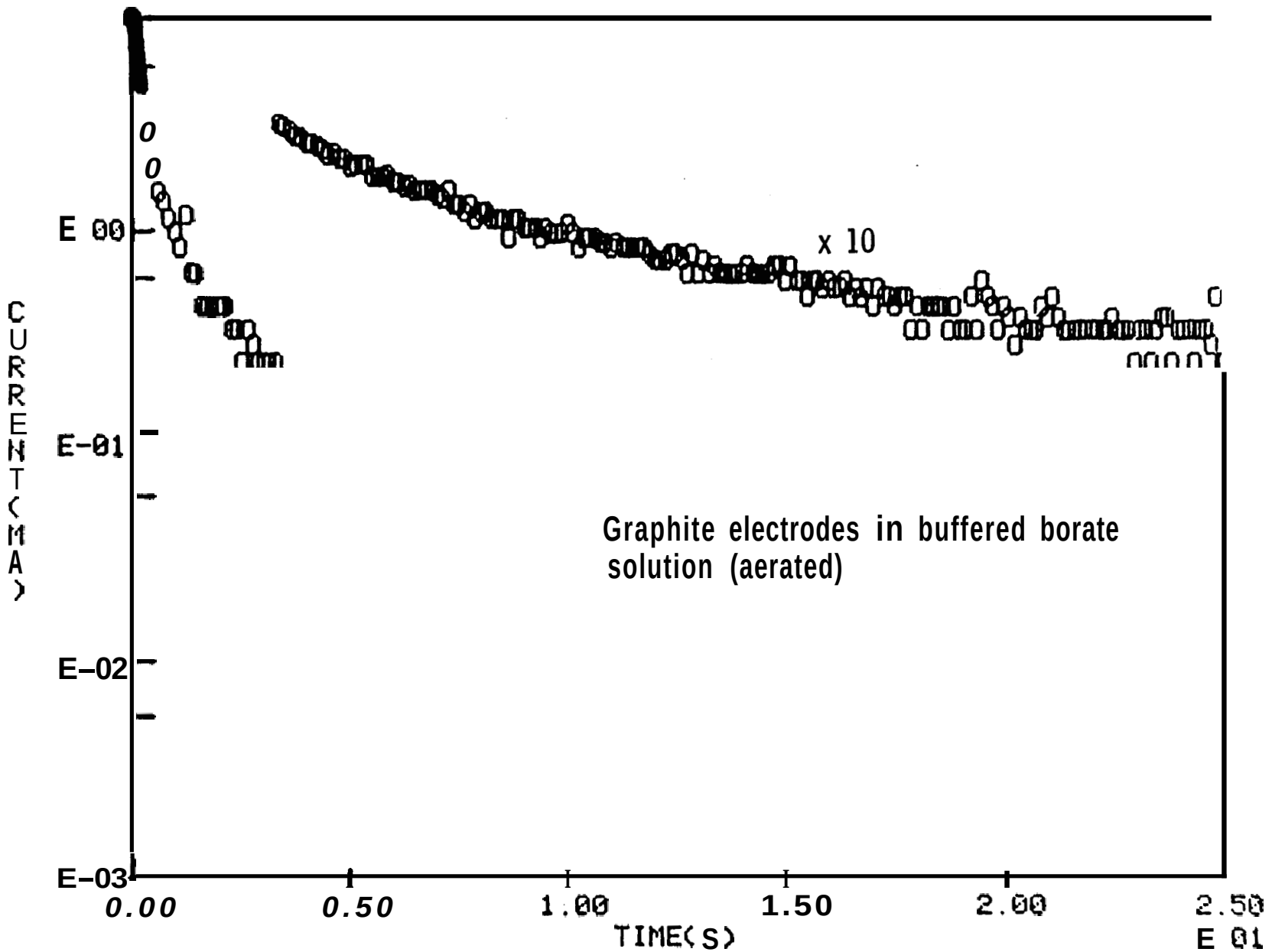

Fig. 5: Typical galvanic current transient between graphite electrode in an aerated buffered solution (pH = 8.8) at room temperature showing the effect of dissolved oxygen.

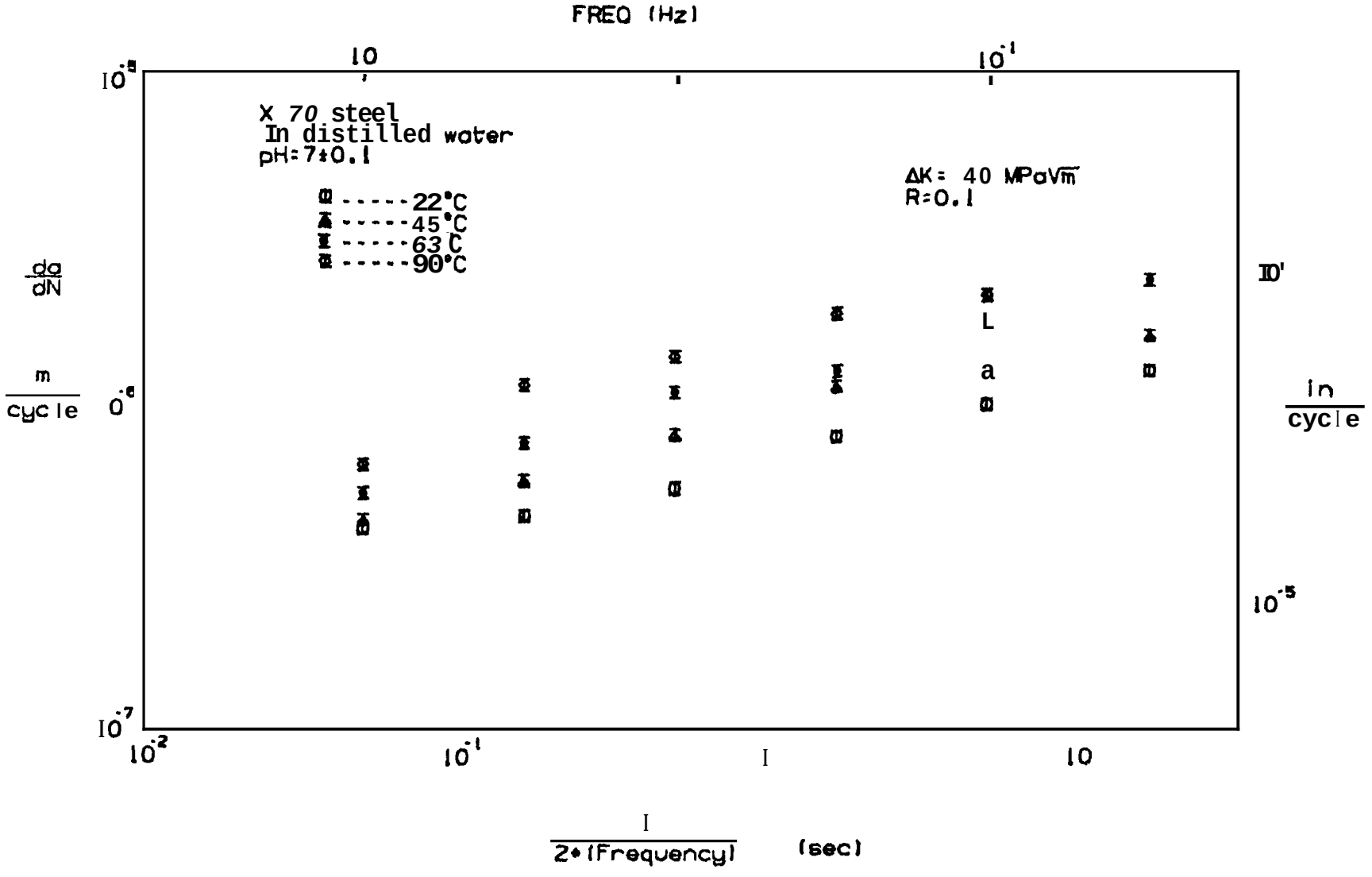

Fig. 6: The influence of frequency on fatigue crack growth for an X-70 steel plate in distilled water at different temperatures (R = 0.1).

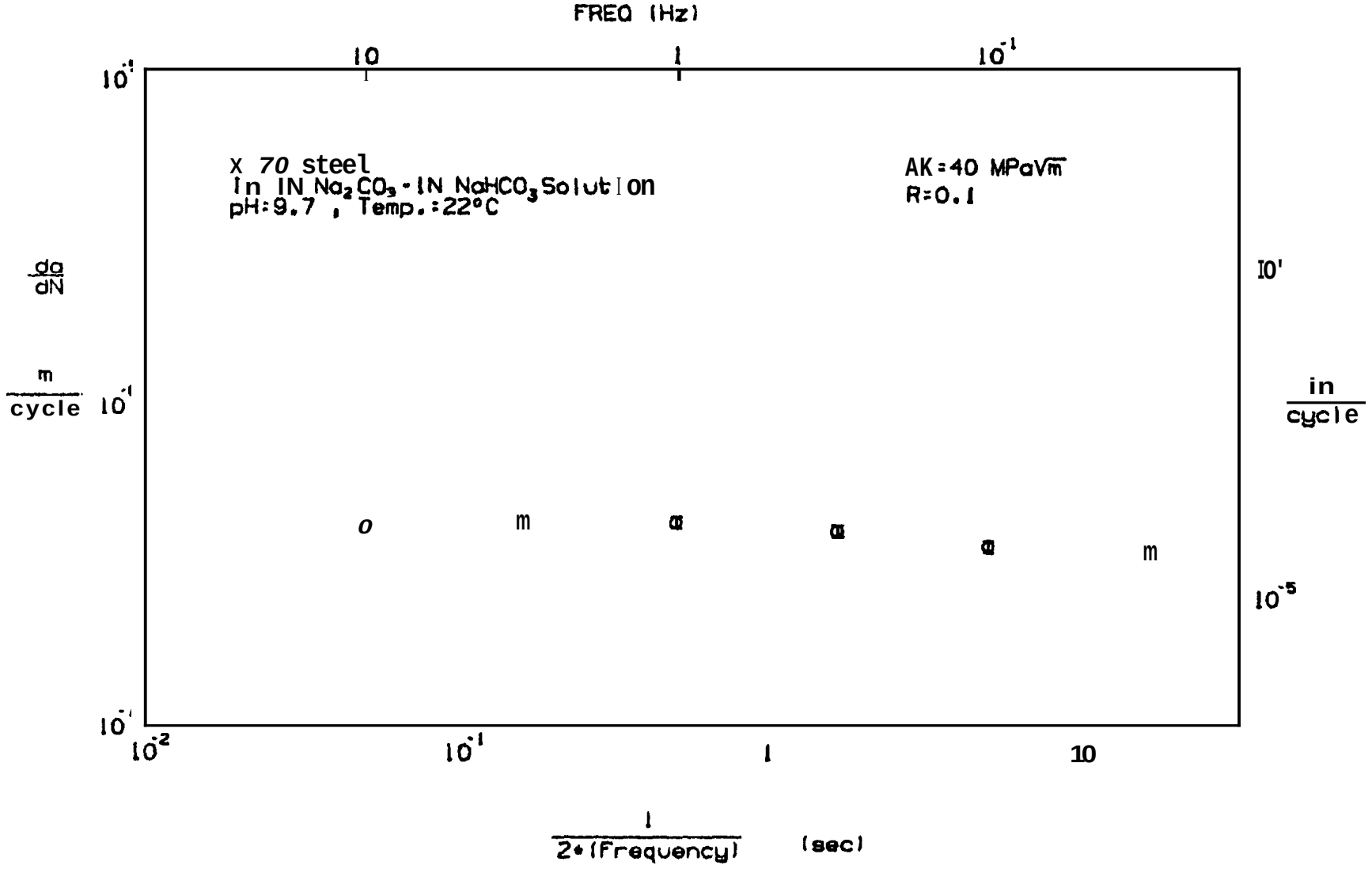

Fig. 7: The influence of frequency on fatigue crack growth for an X-70 steel plate in 1N Na_2CO_3 - 1N $NaHCO_3$ solution at room temperature (R = 0.1).

APPENDIX A

THE CRACK-INCLUSION INTERACTION PROBLEM

1. Introduction

In studying the fracture of multi-phase materials, structures composed of bonded dissimilar solids, and welded joints it is necessary to take into account the effect of the imperfections in the medium. Generally such imperfections are in the form of either geometric discontinuities or material inhomogeneities. For example, in welded joints various shapes of voids, cracks, notches and regions of lack of fusion may be mentioned as examples for the former and variety of inclusions for the latter. From the viewpoint of fracture mechanics two important classes of imperfections are the planar flaws which may be idealized as cracks and relatively thin inhomogeneities which may be idealized as flat inclusions with "sharp" boundaries. In both cases the edges of the defects are lines of stress singularity and, consequently, regions of potential crack initiation and propagation.

The technical literature on cracks, voids and inclusions which exist in the material separately is quite extensive. However, the problems concerning the interaction of cracks, voids and inclusions do not seem to be as widely studied (see, for example, [1] for the results of crack-circular inclusion or void interaction problem and for some references). In this paper the relatively simple problem of an elastic plane containing a crack and an arbitrarily oriented flat elastic inclusion is considered. Of special interest is the examination of the asymptotic stress field in the neighborhood of inclusion ends and the problems of intersecting cracks and inclusions. The basic dislocation and concentrated force solutions are used to formulate the problem [2]. Hence, the formulation can easily be extended to study problems involving multiple cracks and inclusions.

2. Integral Equations of the Problem

The geometry of the crack-inclusion interaction problem under consideration is shown in Figure 1. It is assumed that the medium is under a state of plane strain or generalized plane stress and the in-plane dimensions of the medium are large compared to the lengths of and the distance between the crack and the inclusion so that the effect of the remote boundaries on the

perturbed stress state may be neglected. Thus, the Green's functions for the concentrated forces and dislocations in an infinite plane may be used to formulate the problem. It is further assumed that the inclusion is sufficiently "thin" so that its bending stiffness may also be neglected.

Referring to Figure 1 we consider the stresses and displacements, due to a pair of edge dislocations on the x axis, a pair of concentrated forces on the line θ=constant and the applied loads acting on the medium away from the crack-inclusion region. Let the subscripts d, p and a designate these three stress and deformation states, i.e., let σ_{dij}, σ_{pij} and σ_{aij}, (i,j) = (x,y) or (i,j) = (r,θ), be the stress components due to dislocations, concentrated forces, and applied loads, respectively. The total stress state in the elastic plane may, therefore, be expressed as

$$\sigma_{ij}(x,y) = \sigma_{dij}(x,y) + \sigma_{pij}(x,y) + \sigma_{aij}(x,y), \quad (i,j = x,y) \tag{1}$$

Let us now assume that the dislocations are distributed along a<x<b, y=0 forming a crack. If g(x) and h(x) refer to the dislocation densities defined by

$$\frac{\partial}{\partial x}[u_y(x,+0) - u_y(x,-0)] = g(x) \ , \ a < x < b \ ,$$

$$\frac{\partial}{\partial x}[u_x(x,+0) - u_x(x,-0)] = h(x) \ , \ a < x < b \ , \tag{2a,b}$$

the corresponding stress components at a point (x,y) in the plane may be expressed as

$$\sigma_{dxx}(x,y) = \int_a^b [G_{xx}(x,y,t)g(t) + H_{xx}(x,y,t)h(t)]dt \ ,$$

$$\sigma_{dyy}(x,y) = \int_a^b [G_{yy}(x,y,t)g(t) + H_{yy}(x,y,t)h(t)]dt \ , \tag{3a-c}$$

$$\sigma_{dxy}(x,y) = \int_a^b [G_{xy}(x,y,t)g(t) + H_{xy}(x,y,t)h(t)]dt \ ,$$

where

$$G_{xx} = \frac{2\mu}{\pi(\kappa+1)} \cdot \frac{(t-x)[(t-x)^2 - y^2]}{[(t-x)^2 + y^2]^2} ,$$

$$G_{yy} = \frac{2\mu}{\pi(\kappa+1)} \cdot \frac{(t-x)[3y^2 + (t-x)^2]}{[(t-x)^2 + y^2]^2} ,$$

$$G_{xy} = \frac{2\mu}{\pi(\kappa+1)} \cdot \frac{y[y^2 - (t-x)^2]}{[(t-x)^2 + y^2]^2} ,$$

$$H_{xx} = \frac{2\mu}{\pi(\kappa+1)} \cdot \frac{y[y^2 + 3(t-x)^2]}{[(t-x)^2 + y^2]^2} , \qquad (4a-f)$$

$$H_{yy} = \frac{2\mu}{\pi(\kappa+1)} \cdot \frac{y[y^2 - (t-x)^2]}{[(t-x)^2 + y^2]^2} ,$$

$$H_{xy} = \frac{2\mu}{\pi(\kappa+1)} \cdot \frac{(t-x)[(t-x)^2 - y^2]}{[(t-x)^2 + y^2]^2} .$$

In (4) u and κ are the elastic constants of the medium, μ the shear modulus, $\kappa = 3-4\nu$ for plane strain and $\kappa = (3-\nu)/(1+\nu)$ for plane stress ν being the Poisson's ratio.

Similarly, from the concentrated force solution as given, for example, in [2] the stress components $\sigma_{pij} = S_{ij}$ due to a pair of forces P_x and P_Y acting at the point (x_o, y_o) may be written as

$$S_{xx}(x,y,x_o,y_o) = \frac{1}{2\pi(\kappa+1)} \frac{(A_1+A_2)P_x + (B_1+B_2)P_y}{[(x-x_o)^2 + (y-y_o)^2]^2} ,$$

$$S_{yy}(x,y,x_o,y_o) = \frac{1}{2\pi(\kappa+1)} \frac{(A_1-A_2)P_x + (B_1-B_2)P_y}{[(x-x_o)^2 + (y-y_o)^2]^2} , \qquad (5a-c)$$

$$S_{xy}(x,y,x_o,y_o) = \frac{1}{2\pi(\kappa+1)} \frac{A_3P_x + B_3P_y}{[(x-x_o)^2 + (y-y_o)^2]^2} ,$$

$$A_1 = -2(x-x_o)[(x-x_o)^2 + (y-y_o)^2]$$

$$A_2 = -\kappa(x-x_o)[(x-x_o)^2 + (y-y_o)^2] - (x-x_o)[(x-x_o)^2 - (y-y_o)^2] + 2(y-y_o)^2(x-x_o)$$

$$B_1 = -2(y-y_0)[(x-x_0)^2 + (y-y_0)^2]$$

$$B_2 = +\kappa(y-y_0)[(x-x_0)^2+ (y-y_0)^2]-(y-y_0)[(x-x_0)^2-(y-y_0)^2]-2(x-x_0)^2(y-y_0)$$

$$A_3 = -\kappa(y-y_0)[(x-x_0)^2+(y-y_0)^2]-(y-y_0)[(x-x_0)^2-(y-y_0)^2]-2(x-x_0)^2(y-y_0)$$

$$B_3 = -\kappa(x-x_0)[(x-x_0)^2+(y-y_0)^2]+(x-x_0)[(x-x_0)^2-(y-y_0)^2]-2(y-y_0)^2(x-x_0)$$

(6a-f)

If the inclusion is located along the line $c < r < d$, θ = constant, and if its bending stiffness is neglected, then the following conditions are valid:

$$u_r(r,\theta+0) = u_r(r,\theta-0),\ u_\theta(r,\theta+0) = u_\theta(r,\theta-0)\ ,$$

$$-P_\theta(r,\theta) = \sigma_{\theta\theta}(r,\theta+0) - \sigma_{\theta\theta}(r,\theta-0) = 0\ , \qquad (7a-d)$$

$$-P_r(r,\theta) = -p(r) = \sigma_{r\theta}(r,\theta+0) - \sigma_{r\theta}(r,\theta-0)\ ,\ (c<r<d).$$

Thus, to formulate the problem it is sufficient to consider only the radial component $P_r=p$ of the concentrated force. For $P_\theta=0$ and $P_r=p$ observing that

$$P_x = p\cos\theta\ ,\ P_y = p\sin\theta\ , \qquad (8a,b)$$

and substituting $x_0 = r_0\cos\theta$, $y_0 = r_0\sin\theta$, by using the kernels S_{ij} given by (5) the stress components σ_{pij} are found to be

$$\sigma_{pxx}(x,y) = \frac{1}{2\pi(\kappa+1)}\int_c^d \frac{(A_1'+A_2')\cos\theta+(B_1'+B_2')\sin\theta}{[(x-r_0\cos\theta)^2+(y-r_0\sin\theta)^2]^2}\,p(r_0)dr_0\ ,$$

$$\sigma_{pyy}(x,y) = \frac{1}{2\pi(\kappa+1)}\int_c^d \frac{(A_1'-A_2')\cos\theta+(B_1'-B_2')\sin\theta}{[(x-r_0\cos\theta)^2+(y-r_0\sin\theta)^2]^2}\,p(r_0)dr_0\ , \qquad (9a-c)$$

$$\sigma_{pxy}(x,y) = \frac{1}{2\pi(\kappa+1)}\int_c^d \frac{A_3'\cos\theta + B_3'\sin\theta}{[(x-r_0\cos\theta)^2+(y-r_0\sin\theta)^2]^2}\,p(r_0)dr_0\ ,$$

where the functions A_i', B_i', (i=1,2,3) are obtained from (6) by substituting $x_o = r_o\cos\theta$ and $y_o = r_o\sin\theta$, e.g.,

$$A'(x,y,r_o) = -2(x-r_o\cos\theta)[(x-r_o\cos\theta)^2 + (y-r_o\sin\theta)^2] \ . \qquad (10)$$

Since the stresses σ_{aij} due to the applied loads are known, from (1), (3) and (9) it is seen that once the functions $g(x)$, $h(x)$ and $p(r)$ are determined the problem is solved. These unknown functions may be determined by expressing the stress boundary conditions on the crack surfaces and the displacement compatibility condition along the inclusion, namely

$$\sigma_{yy}(x,0) = \sigma_{dyy}(x,0) + \sigma_{PYY}(x,0) + \sigma_{ayy}(x,0) = 0 \ , \quad (a<x<b),$$

$$\sigma_{xy}(x,0) = \sigma_{dxy}(x,0) + \sigma_{pxy}(x,0) + \sigma_{axy}(x,0) = 0 \ , \quad (a<x<b), \qquad (11a\text{-}c)$$

$$\varepsilon_{rr}(r,\theta) = \varepsilon_{drr}(r,\theta) + \varepsilon_{prr}(r,\theta) + \varepsilon_{arr}(r,\theta) = \varepsilon_i(r), \ (c<r<d)$$

where $\varepsilon_i(r)$ is the (longitudinal) strain in the inclusion. If, for example, the stress state away from the crack inclusion region is given by σ^{∞}_{ij}, $(i,j) = (x,y)$, then the applied quantities in (11) may be expressed as

$$\sigma_{ayy}(x,0) = \sigma^{\infty}_{yy} \ , \ \sigma_{axy}(x,0) = \sigma^{\infty}_{xy} \ ,$$

$$\varepsilon_{arr}(r,\theta) = \frac{1+\kappa}{8\mu}\left[\sigma^{\infty}_{xx}\left(\cos^2\theta - \frac{3-\kappa}{1+\kappa}\sin^2\theta\right)\right.$$

$$\left. + \sigma^{\infty}_{YY}\left(\sin^2\theta - \frac{3}{1+\kappa}\cos^2\theta\right) + \frac{4}{1+\kappa}\sigma_{xy}\sin 2\theta\right] \ . \qquad (12a\text{-}c)$$

We now note that if $p(r)$ is the body force acting on the elastic medium then $-p(r)$ would be the force acting on the inclusion distributed along its length. Thus, the strain in the inclusion may be obtained as

$$\varepsilon_i(r) = -\frac{1+\kappa_s}{8\mu_s A_s}\int_r^d p(r_o)\,dr_o \qquad (13)$$

where μ_s and κ_s are the elastic constants, and A_s is the cross-sectional area of the inclusion corresponding to unit thickness of the medium in z-direction. From the expression of ε_{rr} given by the Hooke's law

$$\varepsilon_{rr} = \frac{1+\kappa}{8\mu}\left(\sigma_{rr} - \frac{3-\kappa}{1+\kappa}\sigma_{\theta\theta}\right) , \tag{14}$$

from (9) and the corresponding stress transformation it can be shown that

$$\varepsilon_{prr}(r,\theta) = \frac{\kappa}{2\pi(1+\kappa)\mu}\int_c^d \frac{p(r_o)}{r_o - r}\, dr_o . \tag{15}$$

Similarly, from (3), (4) and (14) we find

$$\varepsilon_{drr}(r,\theta) = \frac{1+\kappa}{8\mu}\int_a^b [G_\varepsilon(r,t)g(t) + H_\varepsilon(r,t)h(t)]dt \tag{16}$$

where

$$\begin{aligned} G(r,t) = \frac{2\mu}{\pi(1+\kappa)}\frac{1}{R^4}\{&(\cos^2\theta - \tfrac{3-\kappa}{1+\kappa}\sin^2\theta)(t - r\cos\theta)\times \\ &\times[(t-r\cos\theta)^2 - r^2\sin^2\theta] + (\sin^2\theta - \tfrac{3-\kappa}{1+\kappa}\cos^2\theta)\times \\ &\times(t - r\cos\theta)[3r^2\sin^2\theta + (t-r\cos\theta)^2] \\ &t\,\tfrac{4}{1+\kappa}\sin 2\theta\, r\sin\theta[r^2\sin^2\theta - (t-r\cos\theta)^2]\} , \end{aligned} \tag{17}$$

$$\begin{aligned} H_\varepsilon(r,t) = \frac{2\mu}{\pi(1+\kappa)}\frac{1}{R^4}\{&(\cos^2\theta - \tfrac{3-\kappa}{1+\kappa}\sin^2\theta) r\, sine[r^2\sin^2\theta \\ &+ 3(t-r\cos\theta)^2] + (\sin^2\theta - \tfrac{3-\kappa}{1+\kappa}\cos^2\theta) r\ \text{sine}\ \times \\ &\times[r^2\sin^2\theta - (t - r^2\cos^2\theta)^2] + \tfrac{4}{1+\kappa}\sin 2\theta \times \\ &\times(t-r\cos\theta)[(t-r\cos\theta)^2 - r^2\sin^2\theta] , \end{aligned} \tag{18}$$

$$R^2 = (t - r\cos\theta)^2 + r^2\sin^2\theta \quad . \tag{19}$$

Finally, by substituting from (3), (4), (9), (12), (13), (15) and (16) into (11), the integral equations of the problem may be obtained as follows:

$$\frac{1}{\pi}\int_a^b \frac{g(t)dt}{t-x} + \frac{1}{4\pi\mu}\int_C \frac{(A_1'-A_2')\cos\theta+(B_1'-B_2')\sin\theta}{[(x-r_o\cos\theta)^2+(r_o\sin\theta)^2]^2}\, p(r_o)dr_o = -\frac{1+\kappa}{2\mu}\sigma_{YY}^{\infty}\,,$$

$$(a<x<b)$$

$$\frac{1}{\pi}\int_a^b \frac{h(t)dt}{t-x} + \frac{1}{4\pi\mu}\int_C \frac{(A_2'\cos\theta+B_2'\sin\theta)p(r_o)}{[(x-r_o\cos\theta)^2+(r_o\sin\theta)^2]^2}\, dr_o = -\frac{1+\kappa}{2\mu}\sigma_{xy}^{\infty}\,,$$

$$(a<x<b)\,,$$

$$\frac{c_o}{\pi}\int_a^b G_\varepsilon(r,t)g(t)dt + \frac{c_o}{\pi}\int_a^b H_\varepsilon(r,t)h(t)dt + \frac{1}{\pi}\int_C \frac{p(r_o)}{r_o-r}\,dr_o$$

$$+\frac{\gamma c_o}{\pi}\int_C H(r_o-r)p(r_o)dr_o = -\frac{c_o}{\pi}[(\cos^2\theta-\frac{3-\kappa}{1+\kappa}\sin^2\theta)\sigma_{xx}^{\infty}$$

$$+(\sin^2\theta-\frac{3-\kappa}{1+\kappa}\cos^2\theta)\sigma_{yy}^{\infty}+\frac{4}{1+\kappa}\sigma_{xy}^{\infty}\sin 2\theta],\ (c<r<d)\,, \qquad (20a\text{-}c)$$

where

$$c_o = \frac{\pi(1+\kappa)^2}{4\kappa}\,,\quad \gamma = \frac{\mu(1+\kappa_s)}{A_s\mu_s(1+\kappa)}\,. \qquad (21a,b)$$

From the definition of g and h given by (2) it follows that

$$\int_a^b g(t)dt = 0\,,\quad \int_a^b h(t)dt = 0\,. \qquad (22a,b)$$

Also, the static equilibrium of the inclusion requires that

$$\int_C p(r)dr = 0\,. \qquad (23)$$

Thus, the system of singular integral equations must be solved under the conditions (22) and (23). From the function-theoretic examination of the integral equations (20) it can be shown that the unknown functions g, h and p are of the following form [2]:

$$g(t) = \frac{F_1(t)}{(b-t)^{\frac{1}{2}}(t-a)^{\frac{1}{2}}} , \quad h(t) = \frac{F_2(t)}{(b-t)^{\frac{1}{2}}(t-a)^{\frac{1}{2}}} , \quad p(r) = \frac{F_3(r)}{(d-r)^{\frac{1}{2}}(r-c)^{\frac{1}{2}}} ,$$

(24a-c)

where F_1, F_2 and F_3 are bounded functions. The solution of (20) subject to (22) and **(23)** may easily be obtained by using the numerical method described in [3].

3. Stress Singularities

After solving (20) the Modes I and II stress intensity factors k_1 and k_2 at the crack tips x=a and x=b, y=0 which are defined by

$$k_1(a) = \lim_{x\to a} \sqrt{2(a-x)}\, \sigma_{yy}(x,0) , \quad k_1(b) = \lim_{x\to b} \sqrt{2(x-b)}\, \sigma_{yy}(x,0) ,$$

$$k_2(a) = \lim_{x\to a} \sqrt{2(a-x)}\, \sigma_{xy}(x,0) , \quad k_2(b) = \lim_{x\to b} \sqrt{2(x-b)}\, \sigma_{xy}(x,0) ,$$

(25a-d)

may be obtained as follows:

$$k_1(a) = \frac{2\mu}{1+\kappa} \lim_{x\to a} \sqrt{2(x-a)}\, g(x) , \quad k_1(b) = -\frac{2\mu}{1+\kappa} \lim_{x\to b} \sqrt{2(b-x)}\, g(x) ,$$

$$k_2(a) = \frac{2\mu}{1+\kappa} \lim_{x\to a} \sqrt{2(x-a)}\, h(x) , \quad k_2(b) = -\frac{2\mu}{1+\kappa} \lim_{x\to b} \sqrt{2(b-x)}\, h(x) .$$

(26a-d)

The constants k_1 and k_2 are related to the asymptotic stress fields near the crack tips through the well-known expressions (see, for example, [4] and [5]). However, not so well-known is the asymptotic behavior of the stress fields near the inclusions having sharp edges. From (24c) and (7d) it is seen that the shear stress $\sigma_{r\theta}$ has a square-root singularity at the

tip of the inclusion. However, if one is interested in crack initiation around such singular points, one needs to know the direction and the magnitude of the maximum local cleavage stress, This, in turn, requires the investigation of the complete asymptotic stress field near the singular points. By using the basic form of the solution of the related density functions given by (24) and going back to the original stress expressions, the asymptotic stress fields may be developed by following the general techniques described in, for example, [6] or [7].

In an elastic medium containing an elastic line inclusion under plane strain or generalized plane stress conditions, the asymptotic analysis gives the near tip stress field as follows [7](*).

$$\sigma_{YY}(r,\theta) \simeq \frac{k_1}{\sqrt{2r}} \cos\frac{\theta}{2} ,$$

$$\sigma_{xx}(r,\theta) \simeq -\frac{3+\kappa}{\kappa-1} \frac{k_1}{\sqrt{2r}} \cos\frac{\theta}{2} ,$$

$$\sigma_{xy}(r,\theta) \simeq -\frac{\kappa+1}{\kappa-1} \frac{k_1}{\sqrt{2r}} \sin\frac{\theta}{2} , \qquad (27a\text{-}c)$$

where x,y and r,θ are the standard rectangular and polar coordinates, the origin of coordinate axes is at the inclusion tip and the inclusion lies along the negative x axis or along $\theta=\pi$, $r>0$. Equations (27) suggest that similar to crack problems one may define a (Mode I) "stress intensity factor" in terms of the (tensile) cleavage stress as follows:

$$k_1 = \lim_{r\to 0} \sqrt{2r}\, \sigma_{yy}(r,0) . \qquad (28)$$

From (7) by observing that (at the right end of the inclusion)

$$\sigma_{xy}(r,+\pi) - \sigma_{xy}(r,-\pi) = -p(r) , \qquad (29)$$

*) Note the misprints in (4.6) of [7].

in terms of the function $p(x)$ k_1 may be expressed as

$$k_1 = -\lim_{r\to 0} \frac{1}{2}\frac{\kappa-1}{\kappa+1}\sqrt{2r}\, p(r) \ , \tag{30}$$

It should be noted that in the case of flexible elastic line inclusions there is no antisymmetric singular stress field. For example, in a plane under pure shear (σ^{∞}_{xy}) parallel to the inclusion, the perturbed stress field is zero. Physically this of course follows from the fact that the normal strain (ε_{xx}) parallel to the plane of shear is zero.

Similarly, for a rigid line inclusion (i.e., for an inclusion having infinite bending as well as tensile stiffness) it can be shown that for small values of r the asymptotic stress field is given by

$$\sigma_{YY}(r,\theta) \equiv \frac{1}{\sqrt{2r}}\left(k_1 \cos\frac{\theta}{2} + \frac{\kappa+1}{\kappa-1} k_2 \sin\frac{\theta}{2}\right) \ ,$$

$$\sigma_{XX}(r,\theta) \equiv \frac{1}{\sqrt{2r}}\left(-\frac{3+\kappa}{\kappa-1} k_1 \cos\frac{\theta}{2} + \frac{3-\kappa}{\kappa-1} k_2 \sin\frac{\theta}{2}\right) \ , \tag{31a-c}$$

$$\sigma_{XY}(r,\theta) \equiv \frac{1}{\sqrt{2r}}\left(-\frac{\kappa+1}{\kappa-1} k_1 \sin\frac{\theta}{2} + k_2 \cos\frac{\theta}{2}\right) \ .$$

Again, the stress intensity factors k_1 and k_2 are defined in terms of the tensile and shear cleavage stresses at $\theta=0$ plane as follows:

$$k_1 = \lim_{r\to 0}\sqrt{2r}\,\sigma_{yy}(r,0) \ , \ k_2 = \lim_{r\to 0}\sqrt{2r}\,\sigma_{xy}(r,0) \ . \tag{32a,b}$$

As in the crack problems, the antiplane shear component of the asymptotic stress field around flat elastic and rigid inclusions is uncoupled. Defining a Mode III stress intensity factor by

$$k_3 = \lim_{r\to 0}\sqrt{2r}\,\sigma_{xz}(r,0) \ , \tag{33}$$

the asymptotic stress field may be expressed as

$$\sigma_{xz}(r,\theta) \simeq \frac{k_3}{\sqrt{2r}} \cos\frac{\theta}{2} ,$$

$$\sigma_{yz}(r,\theta) \simeq \frac{k_3}{\sqrt{2r}} \sin\frac{\theta}{2} , \qquad (34a,b)$$

where again the inclusion lies along $\theta=\pi$ plane(*).

4. Crack-Inclusion Intersection

Analytically as well as from a practical viewpoint intersection of cracks and inclusions presents some interesting problems. In these problems the point of intersection is a point of irregular singularity with a power other than 1/2. Even though the general intersection problems for an arbitrary value of θ may be treated in a relatively straightforward manner, in this paper only some special cases will be considered.

4.1 The case of $\theta = \frac{\pi}{2}$, $a = 0$, $c = 0$

In this case the system of singular integral equations (20) becomes

$$\frac{1}{\pi}\int_0^b \frac{q(t)}{t-x}\,dt + \frac{1}{\pi}\int_0^d \left[\frac{c_1 t}{x^2+t^2} - \frac{c_2 t x^2}{(x^2+t^2)^2}\right]p(t)\,dt = f_1(x) , \quad (0<x<b) ,$$

$$\frac{1}{\pi}\int_0^b \frac{h(t)}{t-x}\,dt + \frac{1}{\pi}\int_0^d \left[\frac{c_2 x^3}{(x^2+t^2)^2} - \frac{c_1 x}{x^2+t^2}\right]p(t)\,dt = f_2(x) , \quad (0<x<b) ,$$

(*) Note that in this case if the remote stress is decomposed into σ^{∞}_{xz} and σ^{∞}_{yz}, the perturbed stress field due to σ^{∞}_{yz} would be zero, For the cleavage plane θ the shear cleavage stress may be written as $\sigma_{\theta_0}(r,\theta)=\sigma_{xz}\sin\theta-\sigma_{yz}\cos\theta= -(k_3/\sqrt{2r})\sin(\theta/2)$, $\theta_0 = \theta+\pi/2$, indicating that $\theta=\mp\pi/2$ is the maximum cleavage planes.

$$\frac{1}{\pi}\int_0^b \left[\frac{c_3 t}{t^2+r^2} + \frac{c_4 t r^2}{(t^2+r^2)^2}\right] g(t)\,dt + \frac{1}{\pi}\int_0^b \left[\frac{c_3 r}{t^2+r^2} - \frac{c_4 r t^2}{(t^2+r^2)^2}\right] h(t)\,dt$$

$$+ \frac{1}{\pi}\int_0^d \frac{p(t)}{t-r}\,dt + \frac{c_5}{\pi}\int_0^d H(t-r)p(t)\,dt = f_3(r)\ ,\ (0<r<d), \qquad (35a\text{-}c)$$

where

$$c_1 = \frac{3+\kappa}{4\mu}\ ,\ c_2 = \frac{1}{\mu}\ ,\ c_3 = \frac{\mu(\kappa-1)}{\kappa}\ ,$$

$$c_4 = \frac{4\mu}{\kappa}\ ,\ c_5 = \frac{\pi(1+\kappa)(1+\kappa_s)\mu}{4A_s\kappa\mu_s}\ , \qquad (36)$$

and f_1, f_2 and f_3 are known input functions (see, for example, the right hand side of (20)). Note that aside from the simple Cauchy kernels, (35) has kernels which become unbounded as the variables (t,x,r) approach the point of irregular singularity $(x=0=t=r)$. Thus, defining the unknown functions by

$$g(t) = \frac{F_1(t)}{t^\alpha(b-t)^{\beta_1}}\ ,\ h(t) = \frac{F_2(t)}{t^\alpha(b-t)^{\beta_2}}\ ,\ p(t) = \frac{F_3(t)}{t^\alpha(c-t)^{\beta_3}}\ ,$$

$$0<\mathrm{Re}(\alpha,\beta_k)<1,\ (k=1,2,3)\ , \qquad (37a\text{-}c)$$

and by using the function-theoretic technique described in [3], the characteristic equations for β_1, β_2, β_3 and α may be obtained as follows:

$$\cot\pi\beta_k = 0\ ,\ (k = 1,2,3) \qquad (38)$$

$$b_1\cos^2\pi\alpha - (b_2+8\alpha-b_3\alpha^2)\cos^2\frac{\pi\alpha}{2}$$

$$-(b_4-b_5\alpha+b_3\alpha^2)\sin^2\frac{\pi\alpha}{2} = 0\ , \qquad (39)$$

where

$$b_1 = 8\kappa/(1+\kappa)\ ,\ b_2 = 2(3+\kappa)(\kappa-1)/(\kappa+1)\ ,$$
$$b_3 = 8/(\kappa+1)\ ,\ b_4 = 2(3-\kappa)\ ,\ b_5 = 16/(1+\kappa)\ . \qquad (40)$$

Note that the properties of the inclusion (as expressed by the constant c_5 in (36)) enter the integral equations (35) only through a Fredholm kernel and, therefore, have no influence on the singular behavior of the solution, and α is dependent on κ or on the Poisson's ratio of the medium only. From (38) it is seen that the acceptable roots are $\beta_k = 0.5$, $(k = 1,2,3)$. The numerical examination of (39) indicates that in this special case of $e = \frac{\pi}{2}$ we have $0.5<\alpha<1$, meaning that the stress state at $r=0=x$ has a stronger singularity than the conventional crack tip singularity of $1/\sqrt{r}$. This may be due to the fact that in this problem two singular stress fields are combined at $r=0$. Also, it turns out that for $0<\nu\leq.5$ the characteristic equation (39) has two roots in $0<Re(\alpha)<1$ and both are real, These roots are given in Table 1 for various values of the Poisson's ratio.

Table 1. Powers of stress singularity α for a crack and an inclusion: a = 0, c = 0, e = $\pi/2$ (Fig. 1).

v	plane strain		plane stress	
	α_1	α_2	α_1	α_2
0.0	0.63 627093	0	0.63627093	0
0.1	0.64489401	0.09571474	0.64408581	0.08990596
0.2	0.65405762	0.14825371	0.65095281	0.1 3249000
0.3	0.66352760	0.18953334	0.65695651	0.161 76440
0.4	0.67270080	0.22567265	0.6621 7253	0.18404447
0.5	0.67996342	0.26027940	0.66666667	0.20196313

The stress intensity factors at the crack tip x=b, y=0 and at the end of the inclusion x=0, y=d may be obtained by using the relations (26) and (30). At the singular point x=0, y=0 the following useful stress intensity factors are defined;

$$k_1(0) = \lim_{x\to -0} \sqrt{2}\, x^{\alpha}\, \sigma_{yy}(-0,0) \ ,$$

$$k_2(0) = \lim_{x\to -0} \sqrt{2}\, x^{\alpha}\, \sigma_{xy}(-0,0) \ , \qquad (41a,b)$$

for the crack, and

$$k_1(0) = \lim_{y\to +0} \frac{\sqrt{2}}{2}\, y^{\alpha}\, p(0,+0) \qquad (42)$$

for the inclusion.

4.2 The Special Case of $\theta = \frac{\pi}{2}$, $c = -d$, $a = 0$.

In this case the problem is further simplified by assuming "symmetric" external loads (for example, $\sigma^{w}_{xy}=0$ in (20)). Thus, the plane of the crack is a plane of symmetry, $h(x) = 0$, and (20) would reduce to

$$\frac{1}{\pi}\int_{0}^{b} \frac{g(t)}{t-x}\,dt + \frac{2}{\pi}\int_{0}^{d} \left[\frac{c_1 t}{t^2+x^2} - \frac{c_2 t x^2}{(t^2+x^2)^2}\right]p(t)dt = f_1(x), \ (0<x<b) \ ,$$

$$\frac{1}{\pi}\int_{0}^{b} \left[\frac{c_3 t}{t^2+y^2} + \frac{c_4 t y^2}{(t^2+y^2)^2}\right]g(t)dt + \frac{1}{\pi}\int_{0}^{d} \left[\frac{1}{t-y} + \frac{1}{t+y}\right.$$

$$\left. + c_5 H(t-y)\right]p(t)dt = f_3(y) \ , \ (0<y<d) \ , \qquad (43a,b)$$

where, again the input functions f_1 and f_3 are known and, for example, are given in (20) (with $\sigma^{\infty}_{xy} = 0$) and the constants $c_1,\ldots,c_5$ are defined by (36).

By defining

$$g(t) = \frac{G_1(t)}{t^{\alpha}(b-t)^{\beta_1}} \ , \ p(t) = \frac{G_2(t)}{t^{\alpha}(d-t)^{\beta_2}} \ , \ 0<\mathrm{Re}(\alpha,\beta_1,\beta_2)<1 \qquad (44)$$

from (43) it may be shown that

$$\cot\beta_k = 0 \ , \ (k=1,2) \ , \qquad (45)$$

$$\cos\pi\alpha-(c_3 + \frac{1}{2} c_4\alpha)(c_1 - \frac{1}{2} c_2\alpha) = 0 \qquad (46)$$

From (45) it is seen that $\beta_k = 0.5$. A c ose examination of (46) shows that it has only one root for which $0<Re(\alpha)<1$ Furthermore, this root turns out to be real and highly dependent on the Poisson's ratio (see Table 2). The characteristic equation (46) and the roots given in Table 2 are identical to those found in [8] where an infinitely long stringer in cracked plate was considered.

Table 2. Power of stress singularity α at the crack-inclusion intersection for $\theta=\pi/2$, c=-d, a=O and for symmetric loading.

v	α	
	plane strain	plane stress
0	0	0
0.1	0,10964561	0.10263043
0.2	0.17432137	0.15468088
0.3	0.22678790	0.19132495
0.4	0.27392547	0.21972274
0.5	0.31955800	0.24288552

In this problem, too, the stress intensity factors for the crack and the inclusion may be defined as in (41) and (42).

4.3 The Special Case of $\theta=\pi$, a=0, c=0

In this case the crack and the inclusion are on the x axis and occupy $(y=0, 0<x<b)$ and $(y=0, -d<x<0)$, respectively. Restricting our attention again to the symmetric loading for which $h(x) = 0$ and observing that for the variables along the inclusion $r' = -x$, $r_0 = -t$, $p(r_0) = -p_x(t)$, the integral equations of the problem may be expressed as

$$\frac{1}{\pi}\int_0^b \frac{g(t)}{t-x}\,dt - \frac{1}{\pi}\frac{\kappa-1}{4\mu}\int_{-d}^{0} \frac{p_x(t)}{t-x}\,dt = f_1(x)\ ,\ (0<x<b)$$

$$\frac{c_3}{\pi}\int_0^b \frac{g(t)}{t-x}\,dt + \frac{1}{\pi}\int_{-d} \frac{p_x(t)}{t-x}\,dt - c_5\int_{-d}^{x} p_x(t)dt = f_3(x),\ (-d<x<0) \qquad (47a,b)$$

where the constants c_3 and c_5 are defined by (36) and the known functions f_1 and f_3 are given by the right hand sides of (20a) and (20c) (with $\sigma_{xy}^{\infty}=0$). If we now let

$$g(t) = \frac{H_1(t)}{t^{\alpha}(b-t)^{\beta_1}}\ ,\ p_x(t) = \frac{H_2(t)}{(-t)^{\alpha}(t+d)^{\beta_2}}\ ,\ 0<\mathrm{Re}(\alpha,\beta_1,\beta_2)<1\ , \qquad (48)$$

from (47) the characteristic equations for α, β_1 and β_2 may be obtained as follows:

$$\cot\pi\beta_k = 0\ ,\ (k = 1,2)\ , \qquad (49)$$

$$\cos 2\pi\alpha = -\left(\frac{\kappa-1}{2\sqrt{\kappa}}\right)^2\ . \qquad (50)$$

Equation (49) again gives $\beta_1 = \beta_2 = 0.5$. From (50) it may easily be seen that α is complex and its value for which $0<\mathrm{Re}(\alpha)<1$ is found to be

$$\alpha = \frac{1}{2} + i\left(\frac{\log\kappa}{2\pi}\right)\ . \qquad (51)$$

This value of α turns out to be identical to the power of singularity for a perfectly rough rigid stamp with a sharp corner pressed against an elastic half plane having κ as an elastic constant [2] (e.g., $\kappa = 3-4\nu$ for the plane strain case). At first this result may be somewhat unexpected. However, upon closer examination of the problem first, from (47b) it may be seen that the elasticity of the inclusion (i.e., the term containing the constant c_5) has no effect on the nature of the stress singularity. Thus, if one assumes the inclusion to be inextensible, for the symmetric problem under consideration it can be shown that the conditions in the neighborhood of the

crack tip x=0, y=0, for example, for y<0, are identical to the conditions around the corner of the stamp in the elastic half plane occupying y<0. It, therefore, appears that for the elastic inclusion collinear with a crack, the stress state around the common end point would have the standard complex singularity found in the rigid stamp problem.

5. The Results

The crack-incl usion problem described in previous sections is solved for a uniform stress state σ_{ij}^{∞}, (i,j=x,y), away from the crack-inclusion region. For simplicity the results are obtained by assuming one stress component (σ_{xx}^{∞} or σ_{yy}^{∞} or σ_{xy}^{∞}) to be nonzero at a time. The solution for a more general loading may then be obtained by superposition. Even though the stress state everywhere in the plane can be calculated after solving the integral equations (e.g., (20)) and determining the density functions g, h, and p, only the stress intensity factors are given in this section. For nonintersecting cracks and inclusions the stress intensity factors defined by (26) and (28) are normalized as follows:

$$k_i'(x_j) = \frac{k_i(x_j)}{\sigma_a^{\infty}\sqrt{(b-a)/2}} \quad , \quad (i=(1,2);\ x_j=(a,b);\ \sigma_a^{\infty}=(\sigma_{yy}^{\infty},\sigma_{xx}^{\infty},\sigma_{xy}^{\infty})), \tag{52}$$

for the crack and

$$k_1'(r_j) = \frac{k_1(r_j)}{k_o}\ ,\ k_o = \frac{1-\kappa}{2(1+\kappa)}\ \sigma_a^{\infty}\ \sqrt{(d-c)/2}\ ,$$

$$(r_j = (c,d)\ ,\ \sigma_a^{\infty} = (\sigma_{yy}^{\infty},\ \sigma_{xx}^{\infty},\ \sigma_{xy}^{\infty})) \tag{53}$$

for the inclusion.

Referring to Figure 1, for c=a, d=b, and (b/a)=5 the effect of the angle e on the stress intensity factors is shown in Table 3. These results are given for two values of the stiffness parameter γ defined by (21), namely γ=0 (the inextensible inclusion) and γ=10.

Table 3. Normalized stress intensity factors in a plane containing a crack and an inclusion subjected to a uniform stress state σ^{∞}_{ij} away from the crack-inclusion region (c=a, d=b, a=b/5, Fig. 1).

γ	k'	θ						
		1"	30°	60"	90"	120°	150"	180"
		(a) $\sigma^{\infty}_{yy} \neq 0$, $\sigma^{\infty}_{xx} = 0$, $\sigma^{\infty}_{xy} = 0$						
0	$k'_1(a)$	.8905	1.0083	1.0298	1.0049	.9912	1.0001	1.0076
	$k'_2(a)$	-.2152	-.0098	-.0661	-.0830	-.0367	.0004	.0000
	$k'_1(b)$	7.0221	.9967	.9570	.9617	.9857	1.0001	1.0033
	$k'_2(b)$	.4327	-.0065	-.0002	.0007	-.0001	.0001	.0000
	$k'_1(c)$	.9570	-.3273	-1.1324	-1.3970	-.8879	-.0310	.3850
	$k'_1(d)$	.8012	.1552	-.6989	-1.1134	-.7336	.0428	.4320
10	$k'_1(a)$	.9691	.9999	1.0016	.9988	.9978	1.0000	1.0014
	$k'_2(a)$	-.0517	-.0047	-.0136	-.0153	-.0066	.0001	.0000
	$k'_1(b)$	.9862	.9997	.9919	.9928	.9973	1.0000	1.0006
	$k'_2(b)$	.0742	-.0020	.0001	.0005	.0002	.0000	.0000
	$k'_1(c)$	.2619	-.1277	-.3979	-.4735	-.2989	-.0220	.1106
	$k'_1(d)$	-.0269	.1001	-.1848	-.3269	-.2177	.0171	.1354
		(b) $\sigma^{m}_{xx} = \sigma^{\infty}_{xy} = 0$						
0	$k'_1(a)$	.1237	.0704	-.0034	-.0034	.0008	-.0117	-.0203
	$k'_2(a)$	.2355	.0122	.0052	.0310	.0036	-.0161	.0000
	$k'_1(b)$	-.0806	-.0365	.0036	.0142	.0014	-.0072	-.0086
	$k'_2(b)$	-.5321	-.0140	.0001	.0001	.0000	-.0003	.0000
	$k'_1(c)$	-1.1068	-.6949	.0766	.4620	.0774	-.6988	-1.0877
	$k'_1(d)$	-1.4785	-.6941	.0772	.4644	.0776	-.6994	-.0884
10	$k'_1(a)$	.0385	.0106	-.0005	-.0001	.0002	-.0023	-.0038
	$k'_2(a)$	.0587	.0004	.0010	.0056	.0006	.0029	.0000
	$k'_1(b)$	-.0252	-.0068	.0007	.0026	.0003	-.0013	-.0016
	$k'_2(b)$	-.1128	-.0030	.0000	.0000	.0000	.0000	.0000
	$k'_1(c)$	-.3440	-.2152	.0239	.1432	.0239	-.2151	-.3346
	$k'_1(d)$	-.3885	-.2154	.0239	.1434	.0239	-.2151	-.3347

Table 3 - **cont.**

γ	k'	θ						
		1"	30"	60"	90"	120°	150"	180"
		(c) $\sigma^{\infty}_{yy} \neq 0$,						
0	$k'_1(a)$	.1289	.1428	.0669	.0028	.0134	.0223	0.0000
	$k'_2(a)$	1.0849	1.0180	.9054	.9950	1.0599	1.0304	1.0000
	$k'_1(b)$	.1641	-.0754	-.0670	-.0021	0.0231	.0136	0.0000
	$k'_2(b)$	1.4055	.9685	.9974	.9995	1.0005	1.0005	1.0000
	$k'_1(c)$	-1.0246	-1.6348	-1.3085	.0533	7.3767	1.3606	0.0000
	$k'_1(d)$	2.0539	-1.3808	-1.4661	-.1076	1.2735	.3117	.0000
10	$k'_1(a)$	.0858	.0198	.0100	.0010	.0032	.0043	.0000
	$k'_2(a)$	1.0527	.9967	.9826	.9992	1.0108	1.0054	1.0000
	$k'_1(b)$	,1044	-.0140	-.0121	-.0003	.0043	,0025	.0000
	$k'_2(b)$	1.1662	.9929	.9994	.9998	.9999	1.0000	1.0000
	$k'_1(c)$	-.6916	-.5492	-.3731	.0557	.4513	-.4316	.0000
	$k'_1(d)$	1.1639	-.4179	-.4533	-.0342	.3912	-.4029	.0000

Some sample results for an inclusion collinear with a crack (i.e, for $\theta=0$) are given in Table 4. Note that for this configuration under the

Table 4. Normalized stress intensity factors for an inclusion collinear with a crack. Relative dimensions: $\theta=0$, d-c = b-a, c = b+s. Applied loads: σ^{∞}_{ij}, (i,j=x,y). (Fig. 1).

σ^{w}_{ij}	k'	s = (b-a)/100		s = (b-a)/2	
		γ = 0	γ = 10	y = o	y = 10
σ^{w}_{XX}	$k_1'(a)$	-0.0202	-0.0040	-0.001 9	-0.0004
	$k_1'(b)$	-0.1338	-0.0300	-0.0027	-0.0005
	$k_1'(c)$	-1.0482	-0.3296	-1.0889	-0.3347
	$k_1'(d)$	-1.0845	-0.3345	-1.0889	-0.3347
σ^{∞}_{YY}	$k_1'(a)$	1.0047	1.0006	1.0008	1.0002
	$k_1'(b)$	1.0200	0.9987	1.0011	1.0002
	$k_1'(c)$	-0.0861	-0.1571	0.4559	0.1397

loads shown in the table, that is, for σ^{∞}_{YY} and σ^{w}_{xx}, because of symmetry the Mode II stress intensity factors $k_2(a)$ and $k_2(b)$ are zero. Also, for the shear loading σ^{∞}_{xy} it is found that $k_2'(a) = 1$, $k_2'(b) = 1$ and $k_1(a) = k_1(b) = k_1(c) = k_1(d) = 0$. This follows from the fact that in the cracked plane under pure shear σ^{∞}_{xy} the strain component $\varepsilon_{xx}(x,0)$ is zero and hence an inextensible inclusion on the x axis would have no effect on the stress distribution.

Another special configuration is an inclusion parallel to the crack for which Table 5 shows some sample results. In the two special configurations considered in Tables 4 and 5 the effect of the crack-inclusion interaction on the stress intensity factors does not seem to be very significant.

The results for an elastic medium for which xz plane is a plane of symmetry with respect to the crack-inclusion geometry as well as the

Table 5. Nomma ized stress intensity factors in a plane containing an inclusion parallel and equal in length to a crack, both symmetrically located with respect to the y axis. The crack is along the x axis and H is the distance between the crack and the inclusion in y direction (Fig. 1).

a_{ij}^{∞}	k'	H = b-a		H = 10(b-a)	
		y = O	γ = 10	y = o	γ = 10
σ_{xx}^{∞}	$k_1'(a)=k_1'(b)$	-0.0182	-0.0070	-0.0007	-0,0002
	$k_2'(a)=-k_2'(b)$	0.0281	-0.0011	0.0006	0.0000
	$k_1'(c)=k_1'(d)$	-1.0834	-1.0887	-0.0683	-0.0683
5_{YY}^{∞}	$k_1'(a)=k_1'(b)$	1.0063	1.0028	1.0004	1.0001
	$k_2'(a)=-k_2'(b)$	-0.0060	0.0004	-0.0001	0.0000
	$k_1'(c)=k_1'(d)$	0.3917	0.4387	0.0411	0.0276
σ_{xy}^{m}	$k_1'(a)=-k_1'(b)$	-0.0042	0.0000	-0.0002	0.0000
	$k_2'(a)=k_2'(b)$	0.9965	1.0000	0.9998	1.0000
	$k_1'(c)$	-0.11 31	0.0033	-0.0123	0.0004
	$k_1'(d)$	0.1 129	-0.0052	0.0123	-0.0006

applied loads are given in Figures 2-12. .In this example the crack is perpendicular to the inclusion and the external load is a uniform tension parallel or perpendicular to the crack and away from the crack-inclusion region (see the insert in the figures). The results shown in the figures are self-explanatory. However, the solution also has some unusual features among which, for. example, one may mention the tendency of the crack tip stress intensity factors $k'(a)$ and $k'(b)$ to "peaking" as γ decreases and as d/ℓ increases (where $2d$ and 2ℓ are the lengths of the inclusion and the crack, respectively and $\gamma = 0$ corresponds to an inextensible inclusion).

The results for the limiting case of the crack touching the inclusion are given in Figures 8-12. In this case at the singular point $x=0$, $y=0$ the stress intensity factor $k_1(a)$ and the normalized stress intensity factor $k_1'(a)$ are defined by

$$k_1(a) = \lim_{x\to 0-} \sqrt{2}\, x^{\alpha}\sigma_{YY}(x,0) \ , (x < 0) \ , \tag{54}$$

$$k_1'(a) = k(a)/\sigma_{ij}^{\infty}\sqrt{\ell} \ , (i=(x,y);\ \ell=b/2) \tag{55}$$

where the power of singularity α is given in Table 2. The results shown in Figures 8-12 are obtained for $\nu = 0.3$.

The stress intensity factors for the other symmetric crack inclusion problem, namely for the problem in which y axis is the line of symmetry with regard to loading and geometry are given in Figures 13-28. In this problem $a=-a$, $b=\ell$, $d>c>0$ and the external load is either σ_{YY}^{∞} or σ_{XX}^{∞} (see the insert in Figure 13). Note that the figures show the crack tip stress intensity factors at $x=a=-\ell$ and $k_1(b)=k_1(a)$, $k_2(b)=-k_2(a)$. Generally the magnitude of $k_1(a)$ and $k_2(a)$ seem to increase with increasing length and stiffness of the inclusion (i.e., with increasing $(d-c)/2\ell$ and decreasing $\gamma = \mu(1+\kappa_s)/A_s\mu_s(1+\kappa)$, where μ_s is the shear modulus of the inclusion). Also, as expected, $k_1(c)$ and $k_1(d)$ describing the intensity of the stress field at inclusion ends tend to increase as the stiffness of the inclusion increases. However, their dependence on the relative length parameters is somewhat more complicated (see, for example, Figure 16 for change in behavior of the variation of $k_1(d)$ at $(d-c)/2\ell=5$). Figures 13-20 show the effect

of the inclusion length for constant crack length 2ℓ and constant distance c (Figure 13). The effect of the distance c for constant inclusion and crack lengths is shown in Figures 13-28.

The results of the nonsymmetric problem showing the effect of the relative location of the inclusion are shown in Table 6. Referring to Figure 1, in these calculations it is assumed that $e = \frac{\pi}{2}$, $d-c = 2\ell$, $c/2\ell = 0.1$ and $a/2\ell$ is variable.

Finally, the stress intensity factors for the crack-inclusion intersection problem considered in Section 4.1 are given in Figures 29-43. The normalized stress intensity factors shown in these figures are defined by (see (41), (52) and (53))

$$k'_{1B} = \frac{1}{\sigma^{\infty}_{ij}\sqrt{\ell}} \lim_{x\to b} \sqrt{2(x-b)}\, \sigma_{yy}(x,0) ,$$

$$k'_{2B} = \frac{1}{\sigma^{\infty}_{ij}\sqrt{\ell}} \lim_{x\to b} \sqrt{2(x-b)}\, \sigma_{xy}(x,0) ,$$

$$k_{1A} = -\frac{1}{\sigma^{\infty}_{ij}\sqrt{\ell}} \lim_{x\to -0} a\, x^{\alpha}\, \sigma_{yy}(-0,0) ,$$

$$k'_{2A} = \frac{1}{\sigma^{\infty}_{ij}\sqrt{\ell}} \lim_{x\to -0} \sqrt{2}\, x^{\alpha}\, {}_{xy}(-0,0) , \qquad (56)$$

$$k'_{1D} = \frac{1}{k_o} \lim_{y\to d} \sqrt{2(y-d)}\, \sigma_{xx}(0,y) ,$$

$$k_o = \frac{1-\kappa}{2(1+\kappa)}\, \sigma^{\infty}_{ij}\, \sqrt{d/2} \quad .$$

In this case too, generally the magnitude of the stress intensity factors increases with increasing length and stiffness of the inclusion. However, since the crack and the inclusion are located in each other's "shadow", the relative dimensions seem to have considerable influence on the variation as well as the magnitude of the stress intensity factors.

Table 6. The effect of the relative location of inclusion on the stress intensity factors; $\theta = \pi/2$, $(d-c)/2\ell = 1$, $c/2\ell = 0.1$ (Figure 1).

σ^{∞}_{ij}	$\frac{a}{2\ell}$	$k_1'(a)$	$k_2'(a)$	$k_1'(b)$	$k_2'(b)$	$k_1'(c)$	$k_1'(d)$
σ^{∞}_{xx}	0.1	-0.0202	0.0490	0.0161	0.0003	0.4450	0.4471
	0.0	-0.1033	0.0425	0.0133	0.0039	0.4192	0.4402
	-0.1	-0.0849	-0.0044	0.0076	0.0081	0.3538	0.4285
	-0.3	-0.0349	-0.0308	0.0023	0.0060	0.3348	0.4163
	-0.5	-0.0363	-0.0114	-0.0363	0.0114	0.3195	0.4109
σ^{w}_{yy}	+0.1	1.0458	-0.1396	0.9545	0.0012	-1.5217	-1.0543
	0.0	1.2652	-0.1090	0.9667	-0.0078	-1.2922	-0.9497
	-0.1	1.1548	0.0064	0.9865	-0.0150	-0.5345	-0.8136
	-0.3	1.0448	0.0294	1.0013	-0.0102	-0.2308	-0.6378
	-0.5	1.0313	0.0129	1.0313	-0.0129	-0.1959	-0.5801
σ^{∞}_{xy}	0.1	0.0098	0.9905	-0.0033	0.9992	0.1050	-0.1338
	0.0	0.0493	0.9796	-0.0065	0.9983	-0.1734	-0.1675
	-0.1	0.0463	1.0019	-0.0041	0.9960	-0.1054	-0.1648
	-0.3	0.01 23	1.0066	-0.0007	0.9971	-0.0236	-0.0977
	-0.5	0	1	0	1	0	0

References

1. F. Erdogan and G.D. Gupta, "The Inclusion Problem with a Crack Crossing the Boundary", Int. J. of Fracture, Vol, 11, pp. 13-27, 1975.

2. I.N. Muskhelishvili, ~~Some Basic~~ Problems of the Mathematical Theory of Elasticity, Noordhoff, Groningen, The Nether1ands, 1953.

3. F. Erdogan, "Mixed Boundary Value Problems in Mechanics", Mechanics Today, Vol. 4, S. Nemat-Nasser, ed. pp. 1-86, Pergamon Press Inc., 1978.

4. G.R. Irwin, "Analysis of Stresses and Strains Near the End of a Crack Traversing a Plate", J. Appl. Mech., Vol. 24, Trans. ASME, pp. 361-364, 1957.

5. M.L. Williams, "On the Stress Distribution at the Base of a Stationary Crack", J. Appl. Mech., Vol. 24, Trans. ASME, pp. 109-114, 1957.

6. F. Delale and F. Erdogan, "Transverse Shear Effect in a Circumferentially Cracked Cylindrical Shell", Quarterly of Applied Mathematics, Vol. 37, pp. 239-258, 1979.

7. F. Erdogan and G.D. Gupta, "Stresses near a Flat Inclusion in Bonded Dissimilar Materials", Int. J. Solids Structures, Vol. 8, pp. 533-547, 1972.

8. O.S. Yahsi and F. Erdogan, "A Note on the Cracked Plates Reinforced by a Line Stiffener", Engineering Fracture Mechanics, (to appear) 1984.